ISSN 0454－4641

運輸省港湾技術研究所

港湾技術研究所報告

REPORT OF THE PORT AND HARBOUR RESEARCH INSTITUTE

MINISTRY OF TRANSPORT

VOL.37 NO.4 Dec.1998

NAGASE, YOKOSUKA, JAPAN

港湾技術研究所報告（REPORT OF P.H.R.I.）

第 37 巻　第４号（Vol.37, No.４），1998年12月（Dec. 1998）

目　　次（CONTENTS）

REPORT OF THE PORT AND
HARBOUR RESEARCH INSTITUTE
Vol.37, No.4 (Dec., 1998)

Applicability of Dual Face Serpent-type Wave Generator

Tetsuya HIRAISHI *
Katsuya HIRAYAMA *
Haruhiro MARUYAMA *

Synopsis

The dual-face directional random wave maker has been developed in order to reproduce the double peaked two-directional waves composed of swells and wind waves as well as long period waves. The generator is also designed to enlarge the effective test area for target directional waves. The third purpose of the development is the generation of irregular waves with continuously variable propagating direction. The generator consists of two generator faces each installed along one of long and short side wall in the basin. Experimental results from a series of wave generation tests demonstrate that the dual-face serpent-type wave generator system is suitable to reproduce the two directional waves, long period waves and irregular waves of which direction varies time-dependently. The effective test area becomes as large as the whole area of the basin when the principal wave direction is inclined 45° from the both generator faces.

Key Words : Directional random waves, Directional wave generator, Dual-face serpent type wave generator, Experimental test, Long period waves, Multi-face wave generator

*Wave Laboratory, Hydraulic Engineering Division
(3-1-1, Nagase, Yokosuka, Kanagawa, Japan 239-0826, tel:81-468-44-5010, fax:81-468-41-3888,
E-mail hiraishi@cc.phri.go.jp)

港湾技術研究所報告
第37巻第4号(1998.12)

デュアル・フェース・サーペント型造波装置の適用性

平石　哲也*・平山　克也*・丸山　晴広*

要　旨

港湾構造物の主要な外力となる海の波は，本来，様々な方向から来襲する成分波のエネルギーが重畳した多方向不規則波としての性質を有しており，室内の模型実験においても，小型の造波機を直線状に多数並べた多方向不規則波造波装置によって，その再現が試みられてきた．ただし，造波装置の設置面は通常単一で，水槽全域で目標とする多方向不規則波を再現することは困難であり，大型の平面模型実験を多方向不規則波の作用下で実験することは困難であった．一方，最近の現地観測では，お互いの伝播方向が異なるうねりと風波が同時に出現する二方向性の波浪がしばしば出現することが明らかとなっており，二方向波浪の室内における再現の要請が高くなった．また，台風の移動に伴って波向が短時間で変化する現象が現地で観測されており，このような波向の変化を実験水槽内で再現することも必要になった．そこで，水槽の広範囲に目標波が造波できる範囲を造るとともに，二方向波浪を再現でき，さらに時間的に波向が変化する不規則波の再現が可能となるように，２面に多方向不規則波造波装置を備えたデュアルフェース・サーペント型造波装置を開発した．模型実験の結果，新しく開発した造波装置は，実験可能領域の拡大，二方向波浪の再現，長周期波の再現，時間的な波向変化を可能とし，これまでに実験できなかった条件で海洋構造物の特性把握のための実験ができることが判明した．

キーワード：多方向不規則波，多面造波，長周期波，デュアルフェースサーペント，二方向波浪

*水工部波浪研究室
（〒239－0826 横須賀市長瀬３－１－１，電話0468－44－5010，ﾌｧｯｸｽ0468－41－3888，
E－mail hiraishi@cc.phri.go.jp）

CONTENTS

1. Introduction

Various types of the directional random wave generators have been widely developed to reproduce experimentally the wave condition similar to real sea waves. Especially, the recent development of active absorption theories of multi-directional waves (Ito, et al.,1996) has made it possible to install a directional wave generator with three generator faces (multi-face directional wave generator) (Ito, et al.,1996, Hiraishi, et al.,1995). A wide area in the basin is possible to be employed as the effective test area (Funke et al., 1987) by the establishment of multi-face wave generators.

Meanwhile, the recent systematic and large-scale field observation (Nagai et al.,1993) demonstrates that the directional spectrum observed offshore often has two peaks at different directions as shown in **Figure 1.** Each peak direction is usually apart more than 90° each other. Such double-peaked directional waves are considered to be composed of 'wind wave' components with relatively short periods and 'swell' components with long periods. Reproduction of double peaked directional waves is of great importance to carry out experimental study on the stability of offshore structures and navigating ships. A new type directional wave maker has been developed for the generation of double-peaked directional waves as well as the multi-face wave generation with active absorption (Hirakuchi, et al., 1992).

Moreover, long period waves with period longer than swell's become important for estimation of the stability and safety of floating structures and large cargo vessels moored to berths. Because long waves' periods are near to natural periods of the system composed of a ship and mooring ropes, their penetration into harbors may cause large surge motion and breakage of the ropes by resonance (Hiraishi,1997a). Periods of long waves range usually from 50 to 100s in prototype (Hiraishi,1997b). The main energy of long period waves propagates as free waves from the offshore area. A standard spectrum of long period waves has been proposed to estimate the influences of long period waves in harbor planning (Hiraishi,1998).

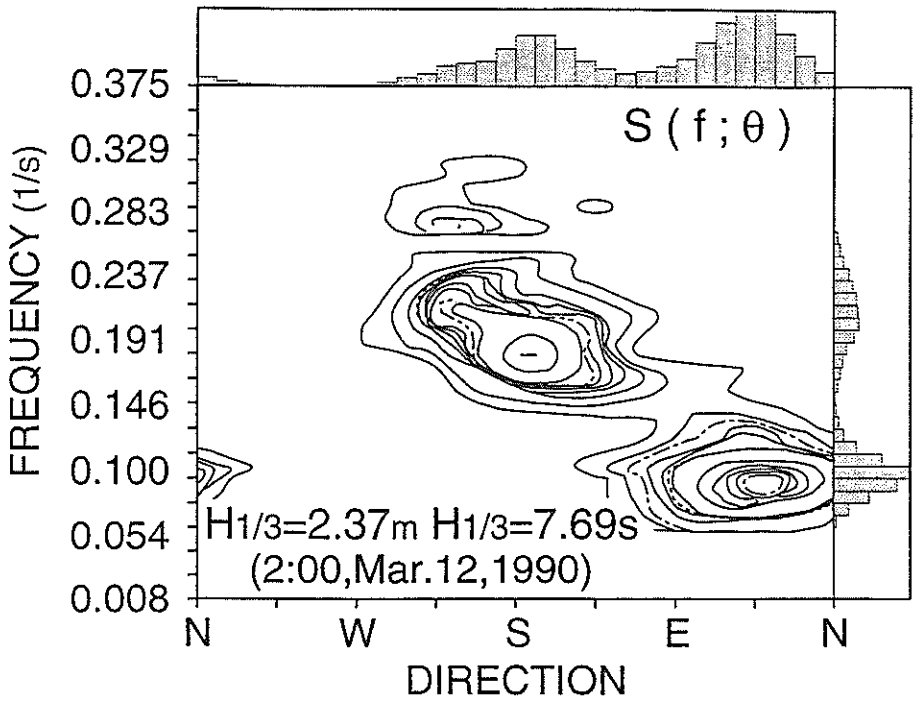

Figure 1 Double-peakd directional spectrum observed in field

Figure 2 shows the proposed profile of a standard spectrum including the short period component (wind wave and swell) and long period wave component. The spectral density of long period wave components are constant and its level is determined by the parameter αl (Hiraishi,1998). The standard spectrum with the parameter αl of 1.60, 1.65 and 1.70 are described in the figure. In order to reproduce the long period components evaluated in the standard spectrum, relatively large strokes are necessary. The newly developed directional wave generator should be also applicable to the generation of combination of short and long period waves because of the maximum stroke of 120cm. The solitary wave approximating tsunami in shallow region is also reproduced employing the long stroke.

The principal wave direction is usually fixed during wave generation. However, the wave direction may vary rapidly and dramatically during one storm and its variation can cause complicated distribution of accumulation and erosion of beach topography in the field. Reproduction of variation on the principal wave direction has to be used in experimental study on litoral drift. The newly developed generator is designed to change the principal wave direction gradually during the course of wave generation. The following section describes the applicability of the newly developed wave generator with segmented piston-type wave paddles.

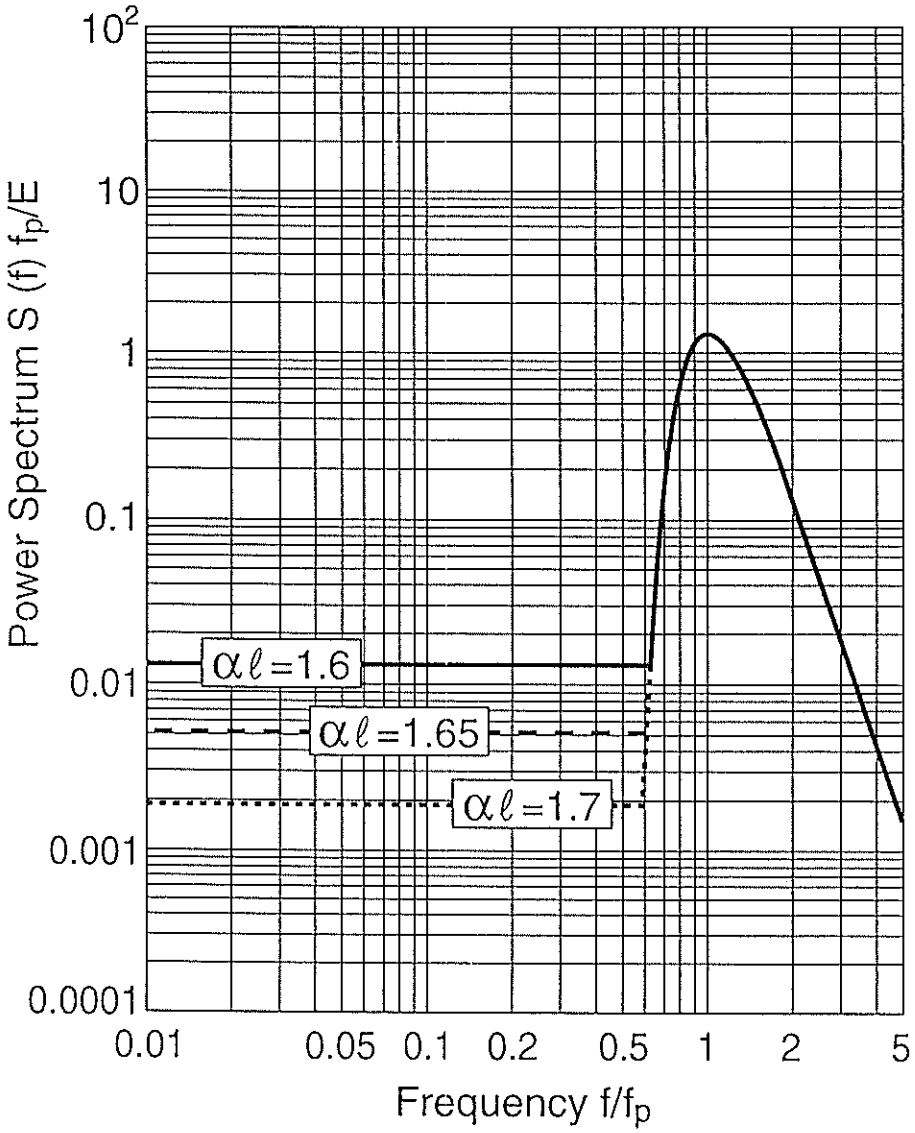

Figure 2 Standard frequency spectrum including long period wave component

2. Frame of Dual Face Serpent-type Wave Generator

2.1 Frame and operation mode of wave generator

Figure 3 shows the conceptional design of the multi-face generator with double faces and with double operation modes. The generator consists of 50 and 30 drive shafts respectively on each side. **Figure 4** shows the cross section of wave maker. The generator is named "Dual face serpent-type wave generator" because of two generator faces. A paddle 130cm heigh is attached between adjoining two drive shafts. Wave paddles are displaced by the mechanical screw shaft system. The maximum water depth and wave height for generation is 100 and 30cm respectively. Each wave paddle is equipped with two wave sensors on its surface to measure the variation of water surface elevation at the front to carry out the active wave absorption for obliquely propagating waves (Ito et al.,1996). The side walls of the basin are covered with the wave dissipating layer composed of the wave energy absorbing material (Takayama et al., 1991). The wave energy absorbing layer is available to prevent waves reflected at the side walls without the generator faces and waves generated backward at the walls with generators.

The generation face indicated below in Fig.3 is named "First face", and the right face "Second face" The wave angle in the basin is defined as the normal propagation angle from the first generation face becomes 0°. The positive direction is counterclockwise. Therefore the wave propagting from the second face normally becomes 90°. **Photograph 1** shows the overview of the dual-face serpent type wave generator.

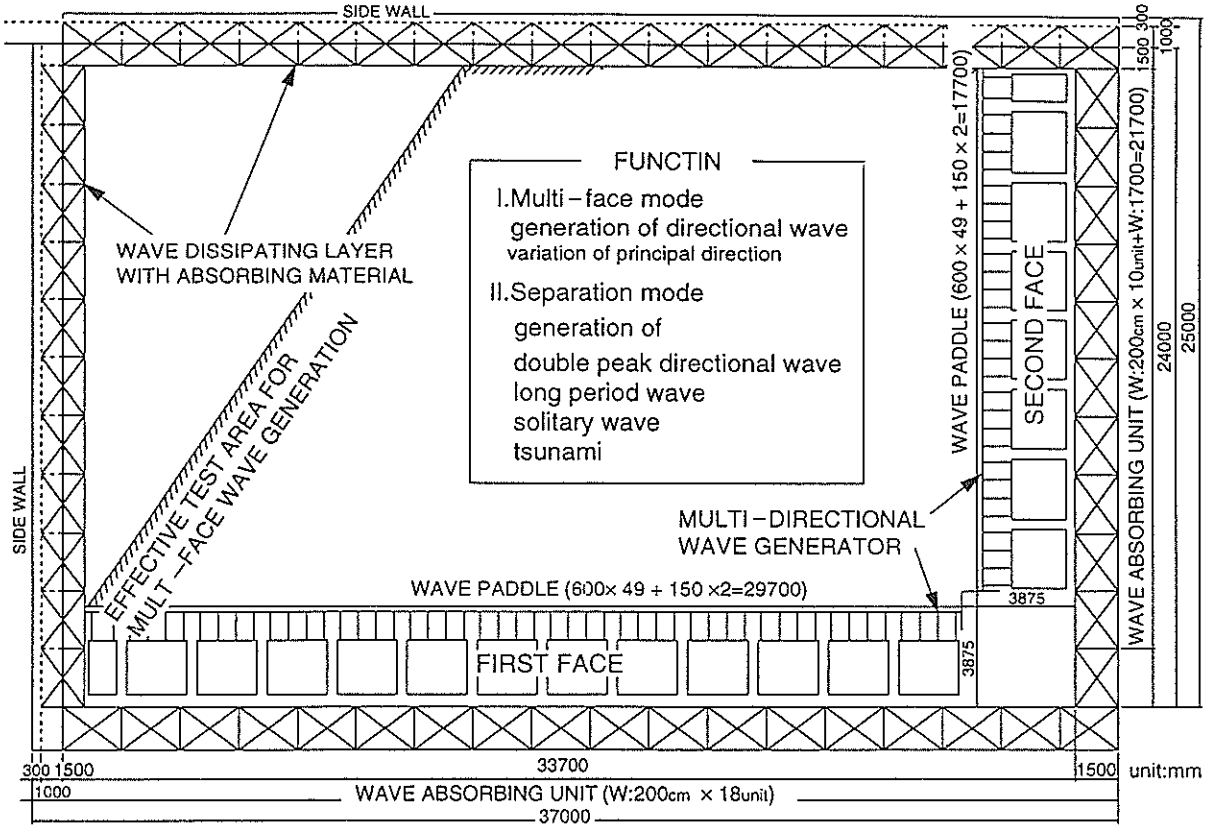

Figure 3 Plane of directional wave basin with dual-face serpent-type generator

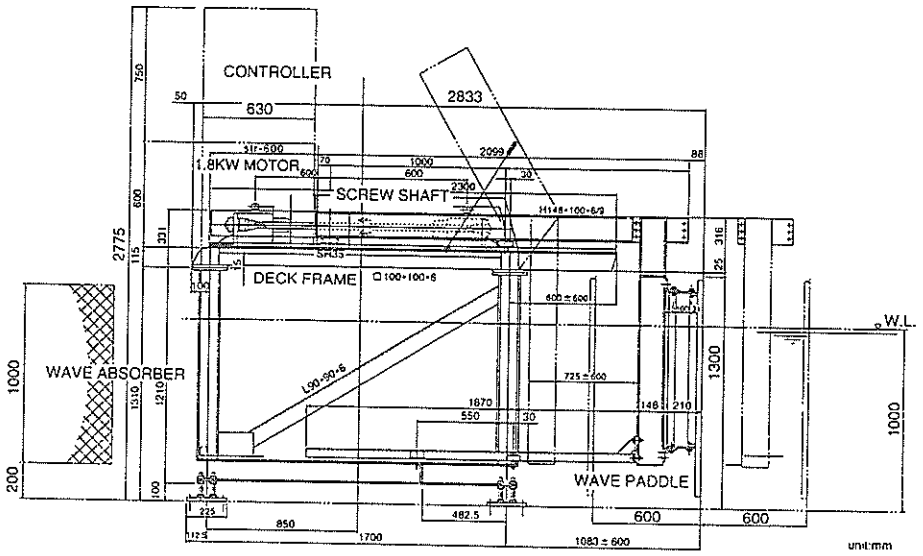

Figure 4 Cross of wave generator unit

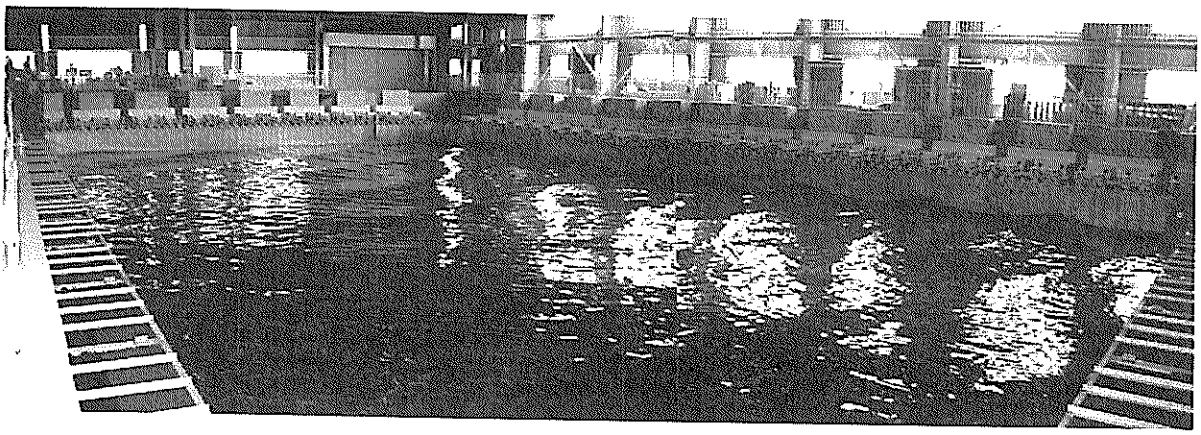

Photograph 1 Overview of dual-face serpent type wave generator

(1) Multi-face mode

The both of first and second faces are operated with the same synthesized signals to make single peaked multi-directional waves. The same target directional wave condition is given to the both faces with different phases. The paddle displacements in the both faces are synthesized according to the single summation model (Takayama and Hiraishi, 1989) for directional wave generation. During operation, the re-reflected oblique wave components from wave paddles are prevented by the active wave absorption motion.

The Bretschneider-Mitsuyasu type frequency spectrum modified by Goda (1987) and the Mitsuyasu-type directional function (Goda,1985) is applied to form the directional spectrum. Directinal spectrum is given generally by,

$$S(f;\theta) = S(f)\ G(\theta;f) \tag{1}$$

The Bretschneider-Mitsuyasu spectrum modified by Goda (1987) $S(f)$ is expressed as,

$$S(f) = 0.205H_{1/3}T_{1/3}(T_{1/3}f)^{-5}\exp[-0.75(T_{1/3}f)^{-4}] \quad (2)$$

where f is the frequency, $T_{1/3}$ significant wave period and $H_{1/3}$ significant wave height. The Mitsuyasu directional function is expressed as,

$$G(\theta;f) = G_0\cos^{2s}((\theta-\theta_p)/2) \quad (3)$$

where θ is the azimuth measured counterclockwise from the principal wave direction θ_p. G_0 is a constant to normalize the directional function.

$$G_0 = \left(\int_{\theta_{min}}^{\theta_{max}} \cos^{2s}\left(\frac{\theta}{2}\right)d\theta\right)^{-1} \quad (4)$$

The indication s represents the energy spreading of directional waves and is determined by the angular spreading parameter S_{max} as follows,

$$s = \begin{cases} S_{max}(f/f_p)^5 & : f \leqq f_p \\ S_{max}(f/f_p)^{-2.5} & : f > f_p \end{cases} \quad (5)$$

where f_p is the peak frequency ($f_p=1/1.13T_{1/3}$). The parameter S_{max} represents the angular spreading parameter (Goda and Suzuki, 1975) which may give the energy concentration to the principal wave direction θ_p. The smaller S_{max} corresponds to the wider spreading of wave energy. Goda and Suzuki (1975) has suggested the parameter S_{max} becomes about 10 for the normal wind waves. The location of wave gage array is included in the effective test area for the first face generator. The effective test area is much larger than the single face directional wave maker. The image of effective test area for the multi-face mode is described in 2.2.

A conecting removable pannel is attached at the corner between the first and second faces. The width of the pannel varies corresponding to the positions of the adjoining paddles in the both faces. The position shifted pannel is proposed to prevent the wave height reduction on the straight line streching from the corner (Hiraishi and Kanazawa,1995). **Photograph 2** shows the overview of the corner connection.

The principal wave direction of target waves is usually fixed to a single direction. However, the wave propagating direction in the sea is sometimes dramatically changed even in a storm because of the rapid traveling of atmospheric low pressures. The variation of wave propagating direction has large influences to the stability of beach. The multi-face mode for generator makes it possible for the principal wave direction to change with any interval during experiment.

(2) Separation mode

Each of the first and second face is operated in the different target wave condition in the separation mode. Therefore, the first face wave maker is available to the generation of directional wind waves with short periods when the second face generates 'swell' with longer periods. For the generation, the both faces are controlled with the active absorption function. The double peaked directional waves are reproduced in the separation mode.

The long period waves with the periods longer than those in swell are generated on the separation mode. A rigid pier was installed at the corner connecting the first and second face. Therefore, no wave is induced due to motion of the corner part. The pier becomes a guide walls to the both faces. In the separation mode, the both faces are applicable to reproduce the directional waves with long period wave components by employing the long driving

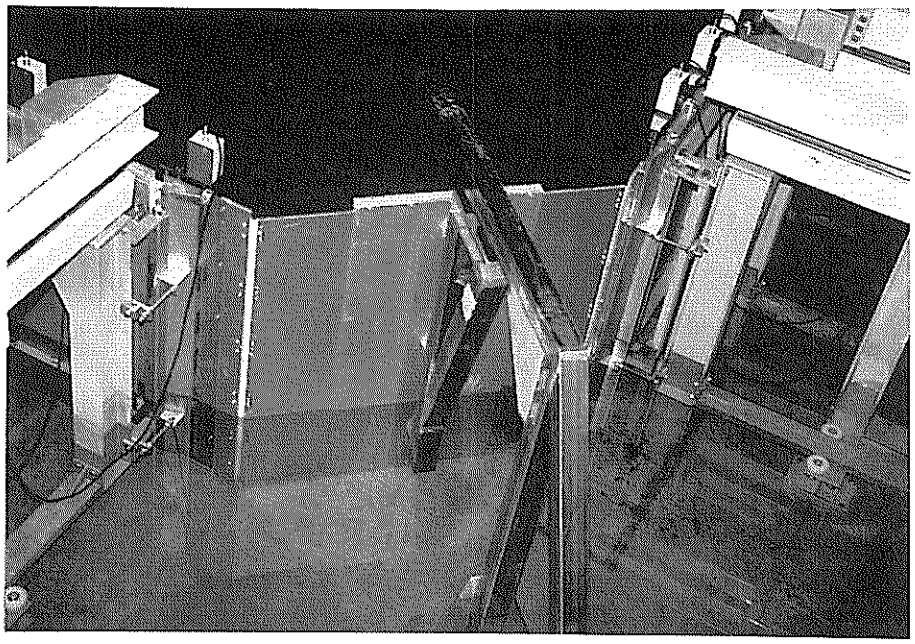

Photograph 2 Removable pannel at corner

shafts of 120cm.

By starting at the most backward paddle position, the second face is available to generate the solitary waves.

2.2 Evaluation of effective test area

The effective test area is defined as the area where the target directional wave is reproduced with good accuracy. Hiraishi and Takayama (1993) suggested the effective test area becomes a triangle with the base line on the generator face in case of a single generator face. **Figure 5** shows the image of effective test area for the case of a single generation face except of influences from the evanescent waves (Takayama, 1982) at the vicinity of generator face. The width of effective test area is very important because the experimental model should be installed inside the area. Therefore, the enlargement of effective test area is innevitable to carry out the experiment for the large size models. The dual-face serpent-type wave maker is applicable to obtain the wide effective test area.

We evaluate roughly the effective test area for the dual-face wave generator. The directional random waves consist of oblique component waves. Therefore, the reproducibility of component oblique regular waves determine the possibility of generation of directional waves. **Figure 6** shows the accumlative curve of directional wave energy proposed by Goda and Suzuki (1975). For the case of $S_{max}=10$, about 80% of total energy is included inside the angle range from -45° to $+45^\circ$. In this case, in order to reproduce the target directional random waves with at least 80% accuracy, the generated wave should include the oblique regular waves of angles from -45° to $+45^\circ$.

Figure 7 shows the image of the effective test area in the dual face directional wave maker. Fig.7 (1), (2) and (3) represents the image of directional wave generation for the principal angle of 0, 30 and 45°. In the figures, the large thick line arrow indicates the target principal wave direction. The thin two vectors correspond to the most inclined component waves. For the generation of directional random waves, the generation of component waves included in the range from the left side to the right side small thin arrow vectors are necessary. For the case of $\theta=0^\circ$, in the region **(i)**, the maximum inclined component wave is indicated in a small arrow with **(f)**. In the rigion, the target directional wave is reperoduced by the motion of the first face**(f)** because every component waves are generated from the first face. For the region **(ii)**, the right side maximum oblique wave component is

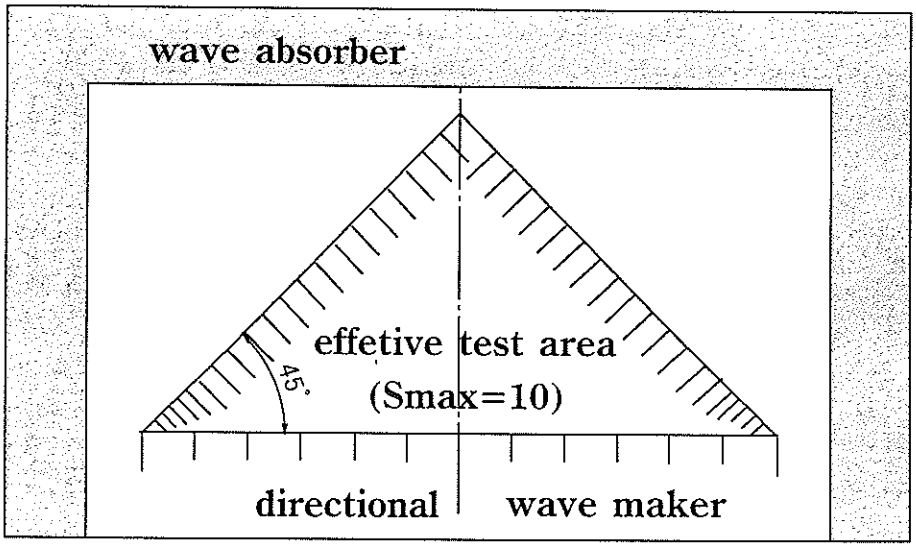

Figure 5 Effective test area for single generation face

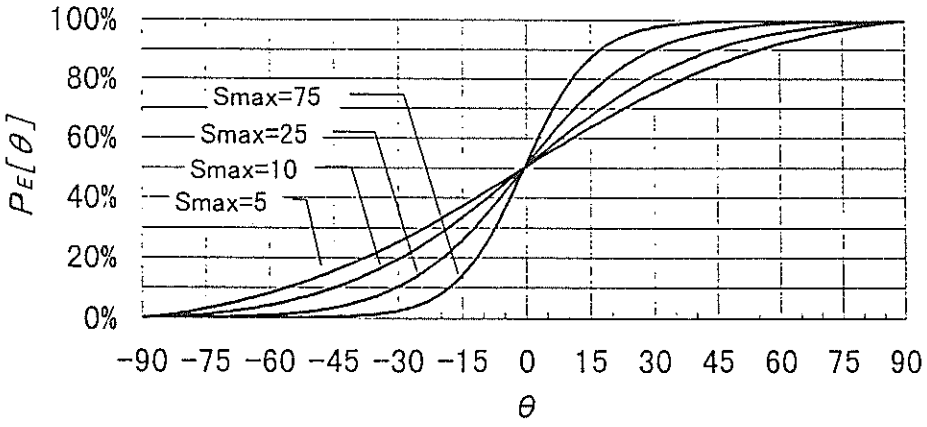

Figure 6 Accumulative curve of directional wave energy

generated from the first face. The left component in the vector figure is not generated from the first face but generated from the second face**(s)**. Therefore, for the case of $\theta p=0^\circ$, the area covered by the region **(i)** and **(ii)** becomes the total effective test area. The boundary of the region **(i)** and **(ii)** is not originally included in the effective test area. However, the boundary region is also included in the effective test area because of the corner connection paddle.

Fig.7(2) shows the image for case of $\theta p=30^\circ$. In the rigion **(i)**, the left side and right side component waves can be reproduced from the first face. For the region **(ii)**, the right components come from the first face while the left side component are reproduced from the second face. The total effective test area becomes the large area surrounded with the thick line.

For the wave principal angle of 45°, the left side component waves are mainly provided from the second face. The components for right side are easily obtained from the motion of first face. In case of $\theta p=45^\circ$, the whole area of basin becomes the effective test area. Therefore, the dual face directional wave generator can be operated most effectively for the case of $\theta p=45^\circ$.

For the principal wave angle of 60° in Fig.7(4), in the rigion **(iii)**, the first face can not provide the oblique waves, therefore all the components are generated from the second surface. In the rigion**(ii)**, the left and right side

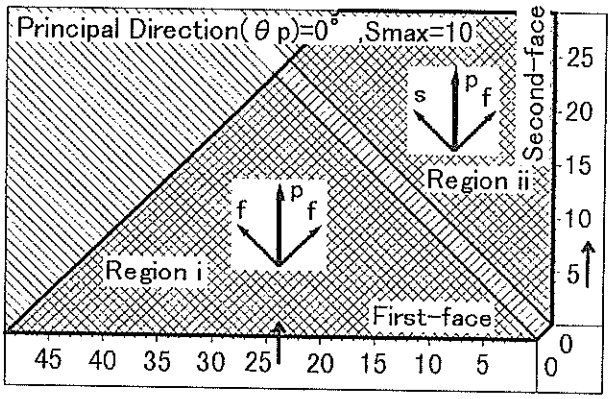

(1) in case of principal direction θp=0°

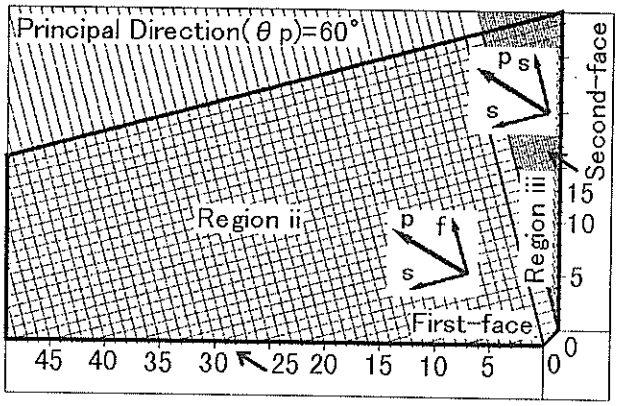

(4) in case of principal direction θp=60°

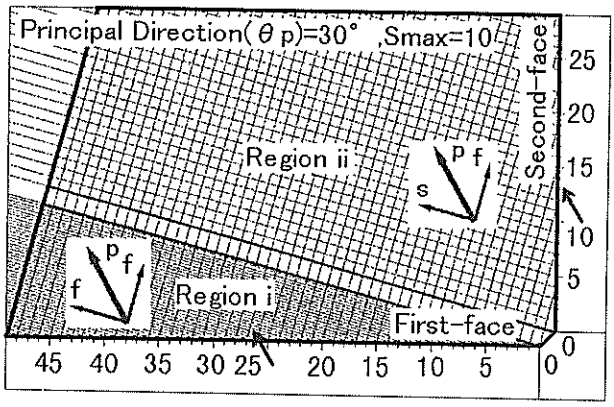

(2) in case of principal direction θp=30°

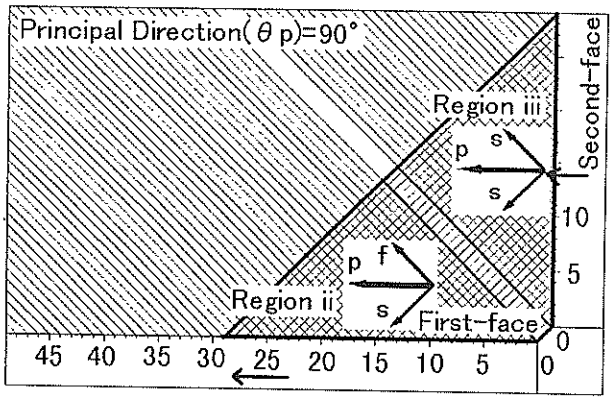

(5) in case of principal direction θp=90°

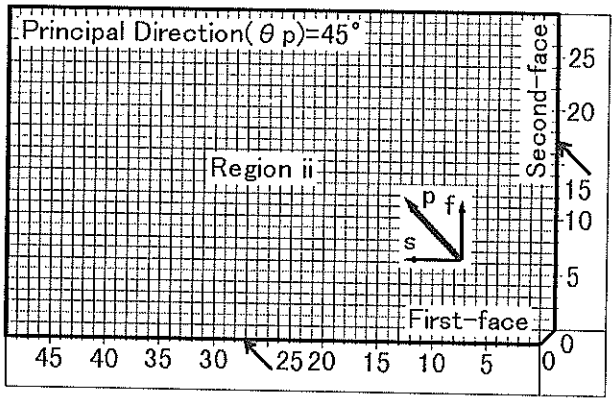

(3) in case of principal direction θp=45°

f : Generated by First-face
s : Generated by Second-face
p : Principal Direction

Figure 7 Image of effective test area for dual-face serpent type wave generator

components are mainly reproduced from the second and first face generator respectively. For the case of $\theta p=90^\circ$ in Fig.7(5), the effective test area corresponds to the sum of the rigion**(ii)** and **(iii)**. The total of effective test area becomes smaller than in the case of $\theta p=45^\circ$. The ranges of required component wave angles for the reproduction of target directional waves depends on the parameter Smax. As shown in Fig.6, the component waves with the angle from -30° to 30° compose the 80% of total wave energy in case of Smax=25.

For the estimation of effective test area except of the case of Smax=10, the diagram consideration similar to the case of Smax=10 is needed to evaluate the effective test area. **Figure 8** shows the results of computation of effective test area in the basin for θp. The original area of the basin is 550m^2. The total effective test area depends on the Smax and the principal wave direction θp. In the figures, the area indicated in the vertical stripe

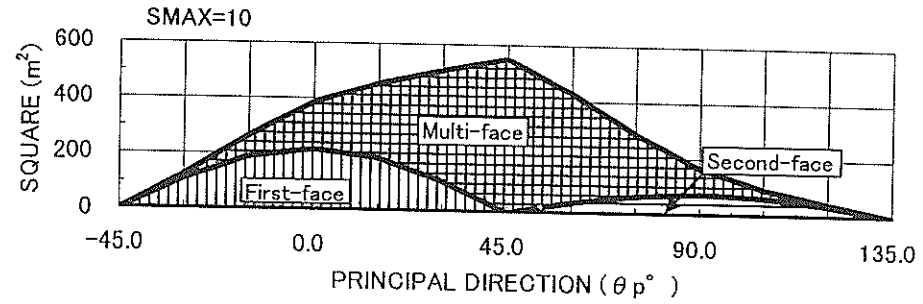

(1) Smax=10

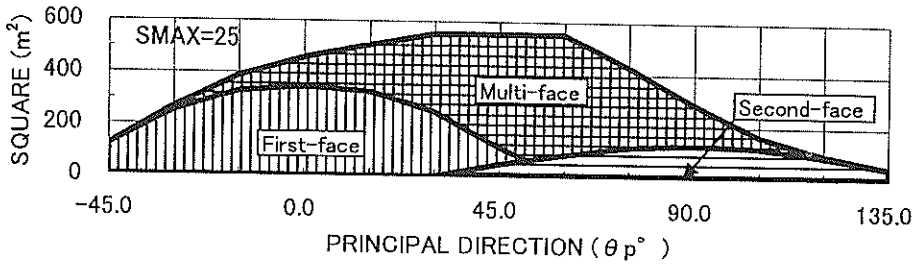

(2) Smax=25

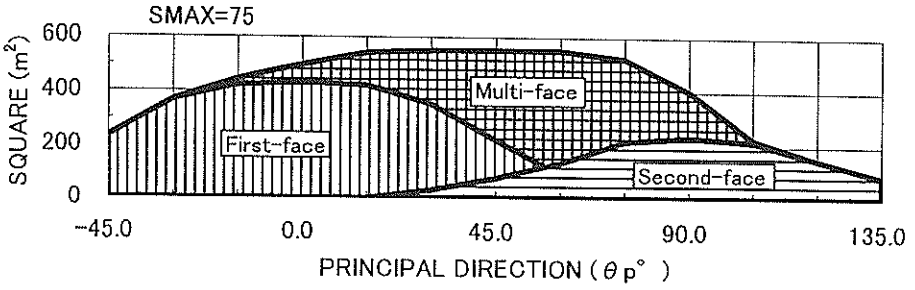

(3) Smax=75

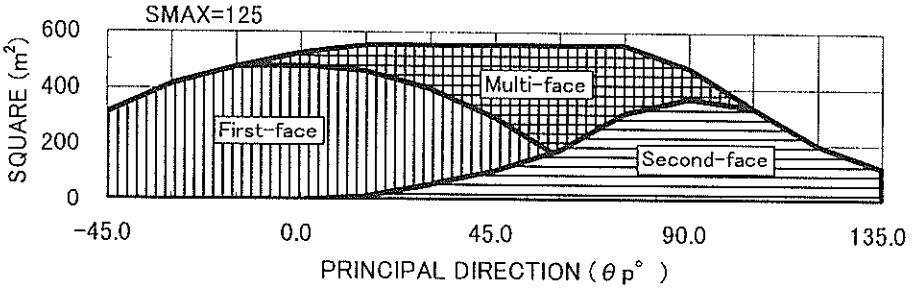

(4) Smax=125

Figure 8 Variation of effective test area for principal wave direction

represents the effective area composed only of the component waves from the first face. The areas for the horizontal stripe represent the region composed only of the componets from the second face. The cross hatched area shows the region where the component waves should be generated from the both of first and second faces.

The total area increases as the parameter Smax becomes large. Moreover, the effective test area becomes maximum when the angle of θp becomes near to 45°. It suggests the dual face directional random wave generator is capable to formate the large effective test area. Especially almost all area of the basin is employed as the effective test area when θp becomes 45°.

3. Experimental Evaluation for Function of Wave Maker

3.1 Absorption of oblique wave

One of the important functions of the generator is the active absorption function to oblique waves. Ito et.al. (1996) has already investigated the applicability of three-point measurement array system for active absorption. We investigated the applicability of the active absorption system of the dual-face serpent type wave generator operated in the separation mode. **Figure 9** shows location of wave gages to measure the incident and reflected wave heights. In the test, the oblique regular waves were generated from the second face.

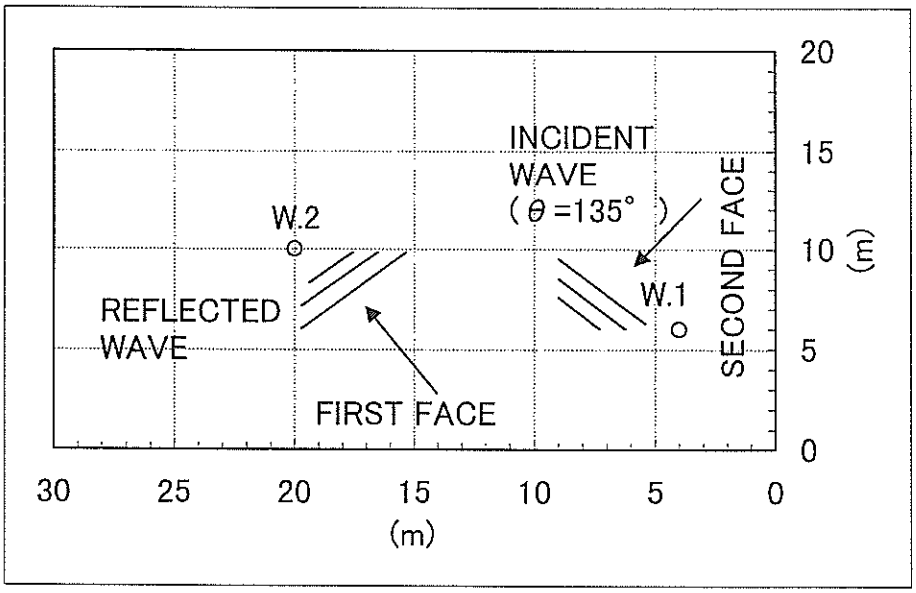

Figure 9 Location of wave gage to measure reflected oblique wave

In the oblique wave absorption test, the angle of waves generated from the second surface became 135°. **Figure 10** shows the wave profiles measured in the wave gages **W.1** and **W.2.** The location of **W.1** is 4m apart from the second face and **W.2** 10m apart the first face as shown in Fig.9. Fig.10(1) and (2) represents the measured wave profiles in the gages **W.1** and **W.2** in the methods without and with the active absorption. In the case without the active absorption function on the first surface, the first surface generator become a simple refelection wall. The wave train represented on the record chart for **W.1** in Fig.10(1) shows a single regular wave group propagating in the basin. The target wave height and period in the generation signal is 5.0cm and 2.0sec respectively. The water depth is 60cm.

In Fig.10(1), the reflected wave height recorded at **W.2** becomes about 3cm at maximum. Therefore, the incident waves are not absorbed on the first face and the almost energy is reflected. The recorded wave train at **W.2** in Fig.10(1) shows the reflected oblique waves for the case without active absorption function. The wave height of reflected waves becomes smaller than those of the generated waves because the energy dispersion by the diffraction. The production of refelected waves from the rigid first surface, however, becomes clear.

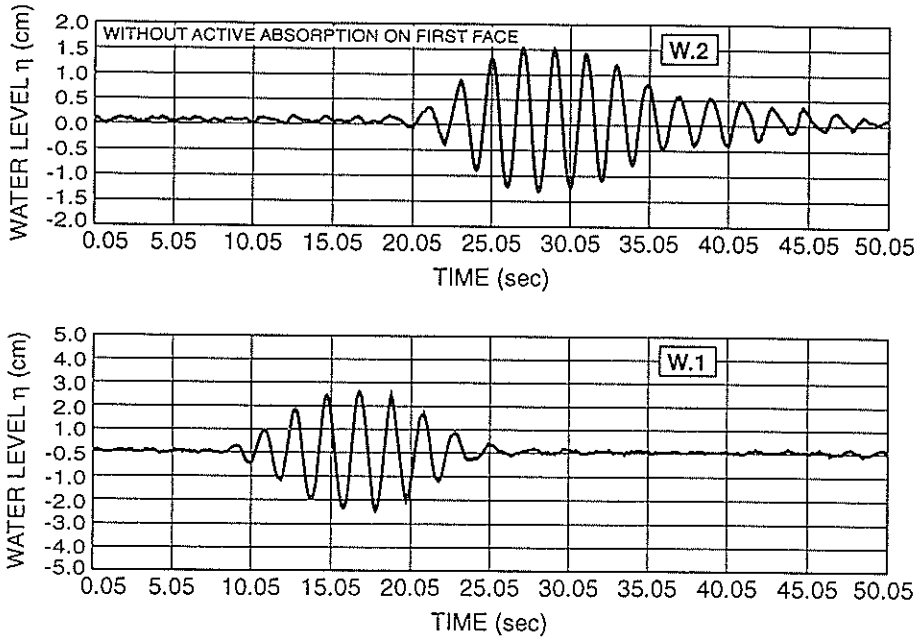

(1) in case without active absorption system

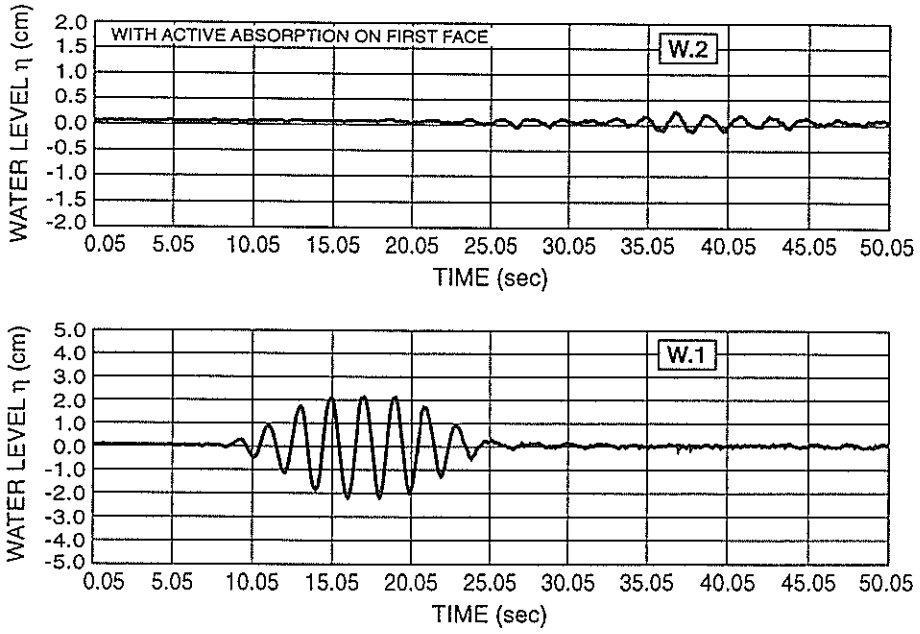

(2) in case with active absorption system

Figure 10 Wave profile of incident and reflected oblique wave

In Fig.10(2) with the active absorption methods, the wave height measured at **W.2** is small. Its height is about 0.5cm in the maximum, which corresponds 10% of the height of waves observed at **W.1.** Therefore, the active absorption function for oblique waves is available to prevent the reflection of oblique incident waves.

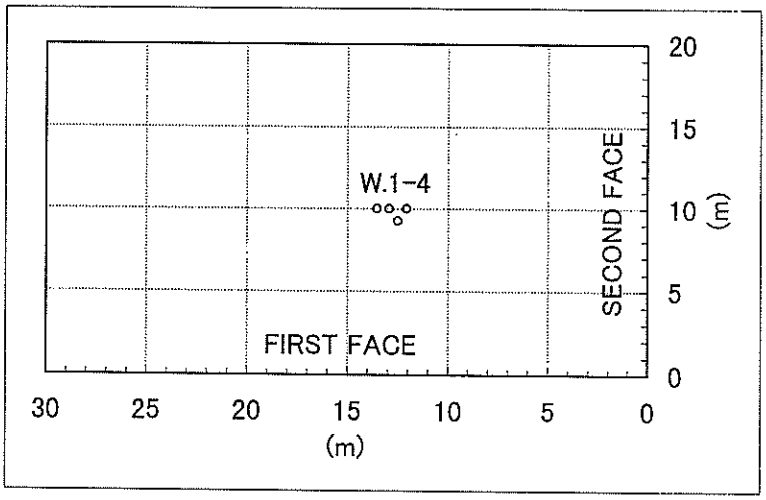

Figure 11 Location of wave gage array to analyze directional wave spectrum

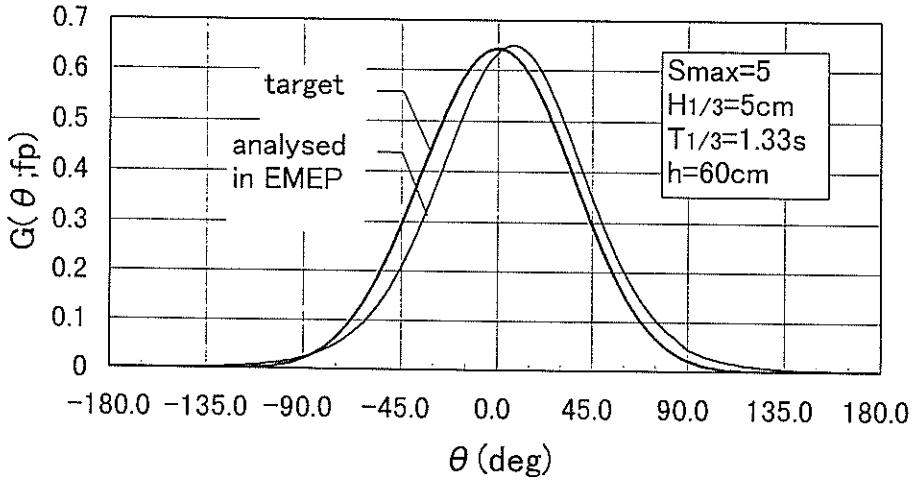

Figure 12 Analyzed directional function at peak frequency

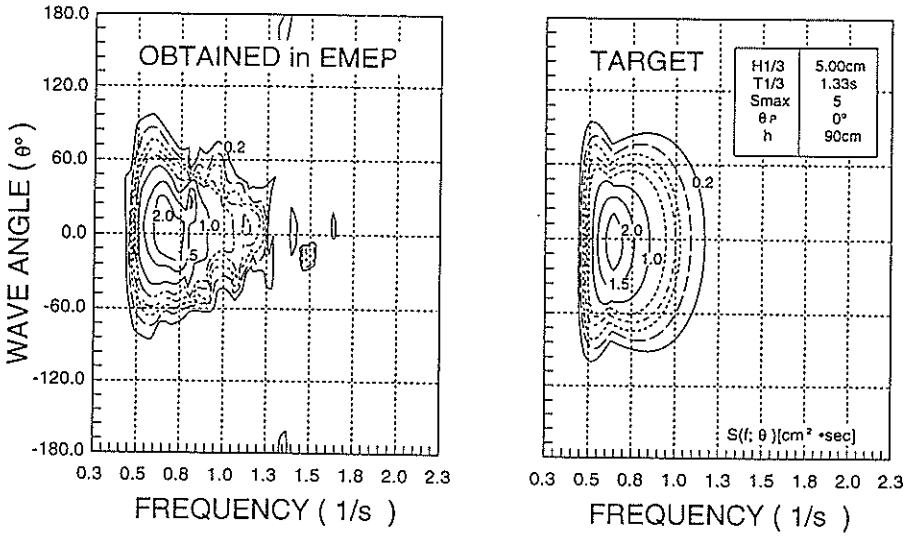

Figure 13 Comparison of measured and target directional spectrum in energy contour map

3.2 Directional waves generated in multi-face mode

Figure 11 shows the arrangement of wave gage array to analyze the directional spectrum. The extended maximum entropy principle (EMEP, Hashimoto et al.,1994) was employed to obtain the directional spectrum from simultaneously measured wave profiles. The location of wave gage array is included in the effective test area for the first surface.

Figure 12 shows the comparison of target and measured directional function at the peak frequency fp. The directional spectral analysis was done in EMEP. The peak value of analysed directional function agrees well with the target. The peak angle slightly differs from the target. The small error in the peak angles may be caused by the slight gap in installation.

Figure 13 shows the comparison of target and experimentally obtained contour maps of directional spectrum at the center of basin for the generation condition of Smax=5. In the figures, the vertical and horizontal axis represents the frequency and wave direction respectively. During generation, the second is working as the wave dissipating layer with the active absorption. If the obliquely propagating components may be reflected at the second surface, the obtained directional function may be distorted by the effect of obliquely reflected waves because of the wide spreading of wave energy with Smax=5. The obtained directional spectrum contour in Fig.13 becomes symmetric, which means the effects by reflection waves are negligible. The obtained wave spectral contour in the left figure becomes similar to the target ones in the right. Therefore, the dual face serpent-type wave generator is applicable to reproduce the directional waves with wider spreading of wave energy.

One of the large advantages to employ the dual-face serpent type wave generator is the possibility to make directional waves with the oblique principal wave direction θ p. The applicability of generation of directional waves with the principal direction of θ p=45° were tested. In order to generate the directional waves of θ p=45°, the appropriate motion of connecting board is inevitable. **Figure 14** shows the comparison of target and obtained directional spectrum in contour expression. The right and left figure represents the target and obtained wave energy contour map respectively. The obtained contour becomes similar to the target one. The peak of spectrum density appears at θ p=45° at the both cases of target and obtained contours.

We compared the directional function at the peak frequency to have a detail check of the principal wave direction. The input parameter Smax for synthesizing wave signal is 25. **Figure 15** shows the directional function at the peak frequency fp of the target and obtained directional waves. In the figure, the profiles analysed in EMEP and in Extended Maximum Likelyfood Method (EMLM, Isobe,1988) is indicated in the dot and broken line respectively. The directional function profile analysed in EMEP agrees with the target one indicated in the solid line. Meanwhile, the profile analysed in EMLM shows the peak lower than the target. The method of EMEP is more appropriate to obtaine the directional spectrum from the wave data simultaneaously measured in a wave gage array than the mehod of EMLM. The peak angle of obtained directional function agrees well to the target of 45°. The multi-mode operation of the serpent type wave generator is applicable to generate the directional waves with the oblique principal wave direction expressed as θ p=30°,45° and so on.

3.3 Reproducibility of directional waves in effective test area

As shown in Fig.8, the whole area of the basin becomes the effective test area when the principal wave angle is 45°. So, we experimentally investigated if the dual face directional wave generator is capable to provide the most large effective test area in case of θ p=45°. For the investigation, the measurement and analysis of directional waves should de carried out in large area. **Figure 16** shows the position of array composed of four sensors in the basin. In the test, the generation of directional waves with the principal direction of θ p=45° with active absorption method was carried out because the effective test area becomes maximum in case of θ p=45°. Four sets of wave gage arrays are installed at **P.1**, **P.2**, **P.3** and **P.4**.

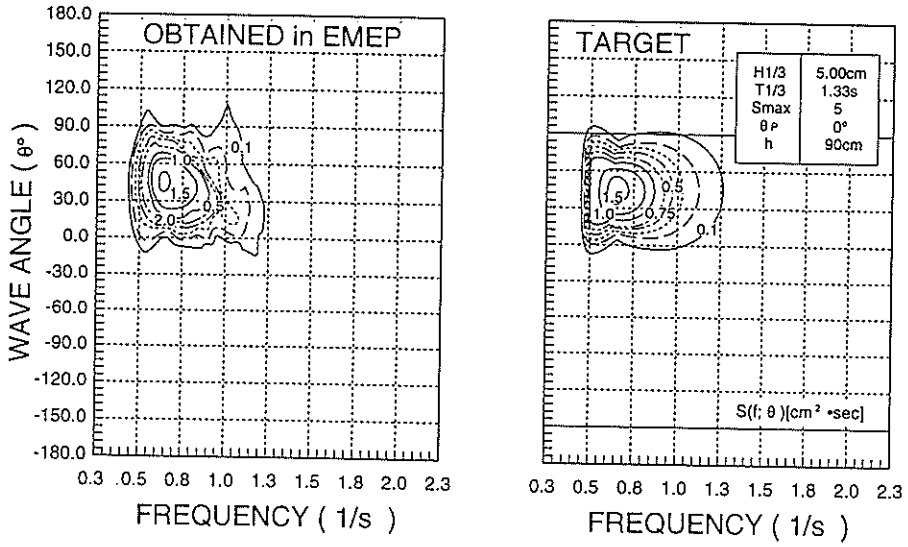

Figure 14 Measured and target directional spectrum in energy contor map for wave with obliqueprincipal wave direction

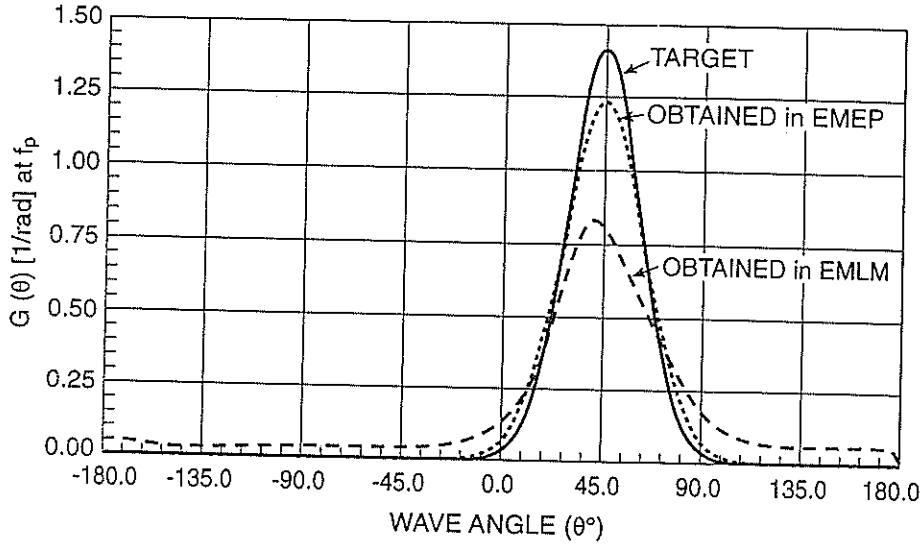

Figure 15 Comparison of directional function at peak frequency f_p of measured and target waves with oblique principal direction

Figure 17 shows the experimental results for frequency spectrum and two dimensional directional spectrum. In the figures, the two-dimensional directional spectrum is represented. The two dimensional directional spectrum is given by,

$$G_2(\theta)=\int_0^\infty S(\theta;f)df \tag{6}$$

In the all measurement points, the frequency spectrum agrees with the target spectrum. At **P1**, **P2** and **P4**, the directional spectrum analysed in EMEP also agrees well with the target profiles. At **P3**, the obtained directional spectrum profiles slightly differs from the target. The disagreement at **P3** may be caused by the influences from the energy dissipation of wave basin on wave propagating. However, the peak angle agrees well with the target.

Therefore, the target wave directionality are reproduced with good accuracy in the whole region.

Figure 18 shows the contour expression of directional spectrum. The peak energy level at the contour map at **P1**, **P2** and **P4** agrees each other and the values is about 5.00 and it is same to the target. The peak value are slightly smaller in the position of **P3.**

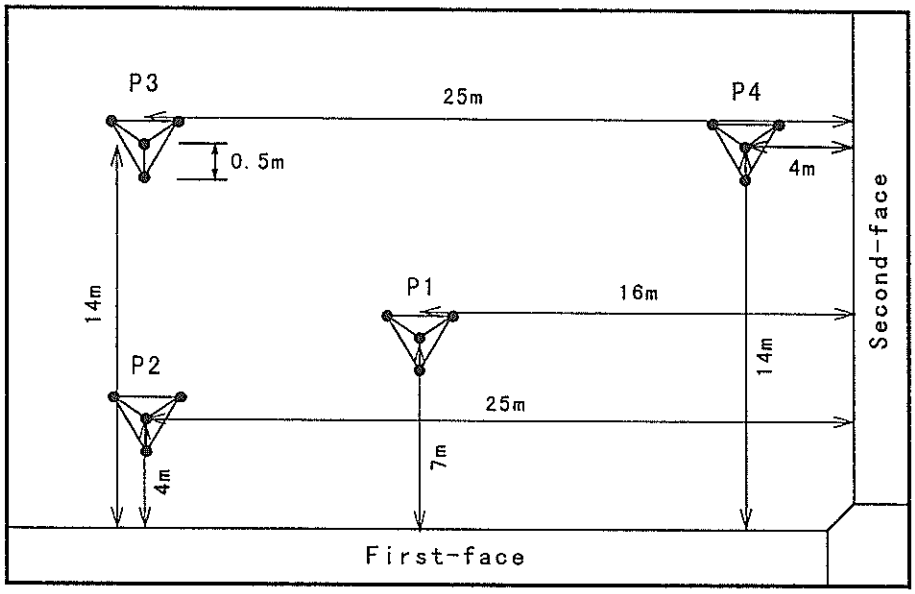

Figure 16 Location of wave gage array for confirmation of effective test area

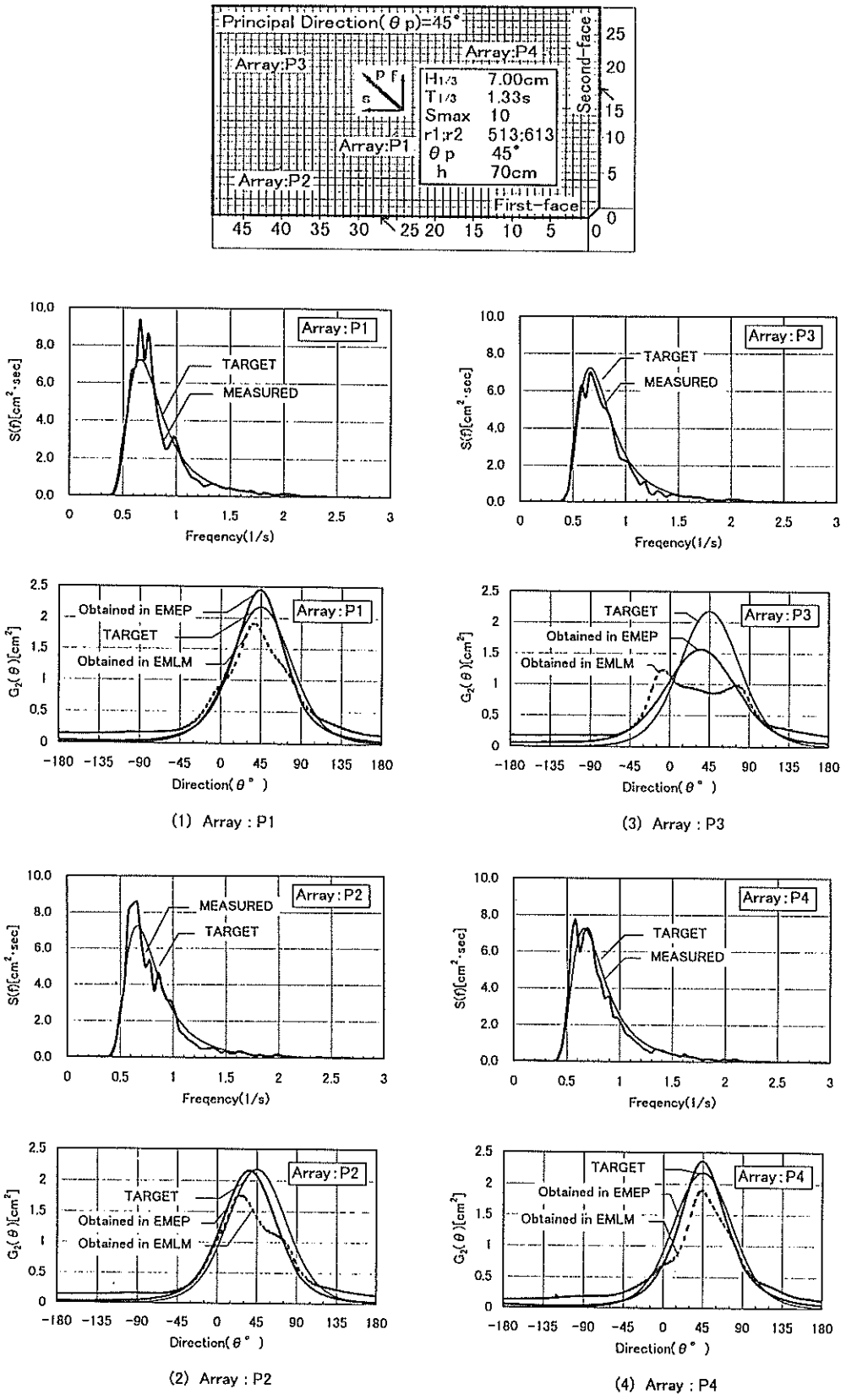

Figure 17 Comparison of two dimensional directional and frequency spectrum in experimental basin with principal wave direction of θ p=45°

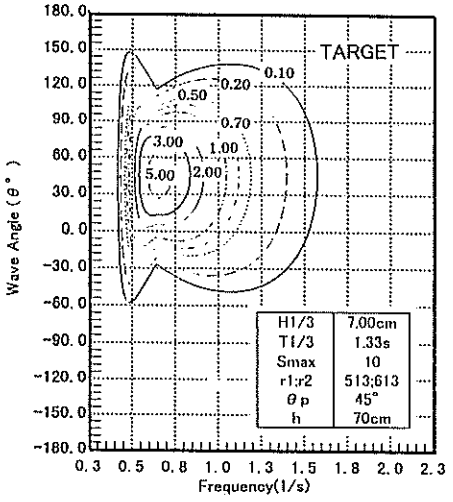

(1)Target

r1: Initial Random Numbar of Frequency
r2: Initial Random Numbar of Direction

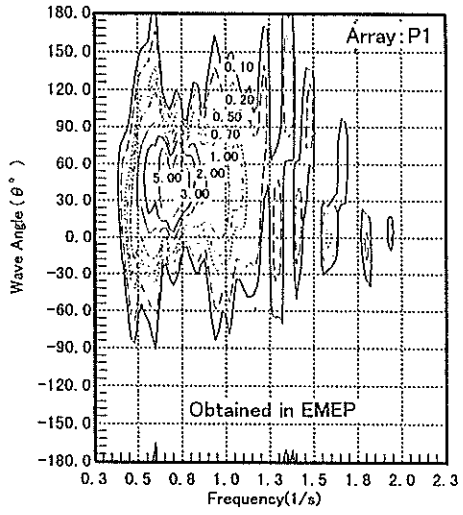

(2)Array:P1

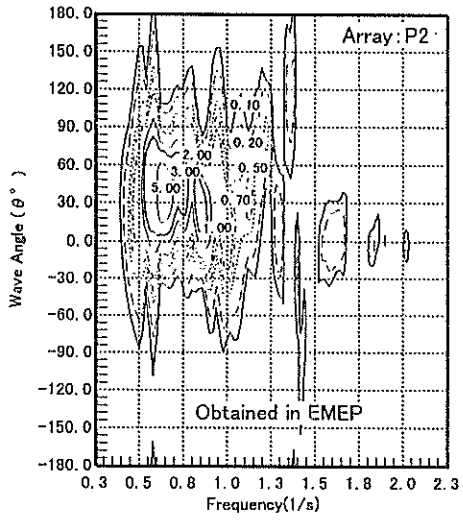

(3)Array:P2

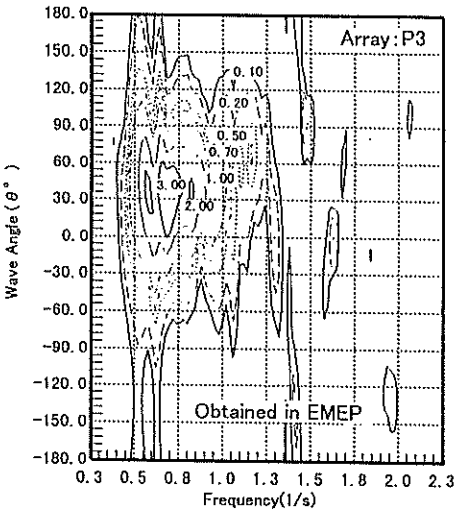

(4)Array:P3

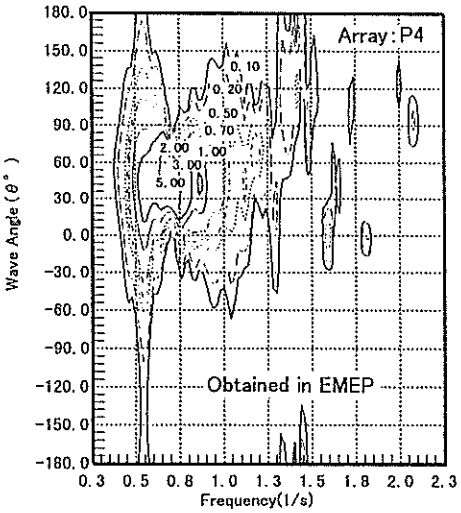

(5)Array:P4

Figure 18 Directional spectrum profiles at different measurement point in basin

3.4 Reproducibility of double-peaked directional wave

In the evaluation tests, the wind waves are generated by the first-face and the swell by the second face. The propagating angle of wind waves and swell is 0° and 90° respectively. The target period of generated wind waves and swells are 1.33 and 2.0sec respectively. **Figure 19** shows the measured two dimensional directional spectrum at the basin center. The target conditions of wind wave and swell components is indicated as 'WAVE-1' and 'WAVE-2' respectively in the upper left side table in the figure.

The profile analysed in EMEP has peaks at the same to the target angles. The energy level of swell components at θ =90° is slightly smaller than the target. In the wind wave components generated by the first surface, the obtained peak angle and energy level agrees well with those of target spectrum. Therefore, the double-peaked directional waves can be reproduced with good accuracy in the dual-face directional wave generator.

Figure 20 shows the comparison of the directional function at the peak frequency of swell components. The directional function's peak angle and energy level agree with those of target respectively. For the wind wave components, the peak angle slightly differs from the target, however, the deferences less than 20°. Considering the directional function at peak frequency, the dual-face serpent type generator is expected to be applicable to genarate double-peaked random waves.

Figure 21 shows the frequency spectrum measured at the center part of the basin. In the case, the target significant wave period for wind wave and swell is 1.0 and 2.0s respectively. In the figure, the target frequency spectrum is represented in the solid line and the obtained by the broken line. The frequency spectrum of generated waves agrees well with the target spectrum and they have spectral profiles with two peaks typically observed in the double-peaked directional wave condition in the field (Nagai et. al.,1993). The good agreements in the directional function and frequency spectrum profiles between the measured and target double-peaked directional waves demonstrate the possibility of the generator to reproduce the complicated sea condition composed of wind waves, swells and long period waves.

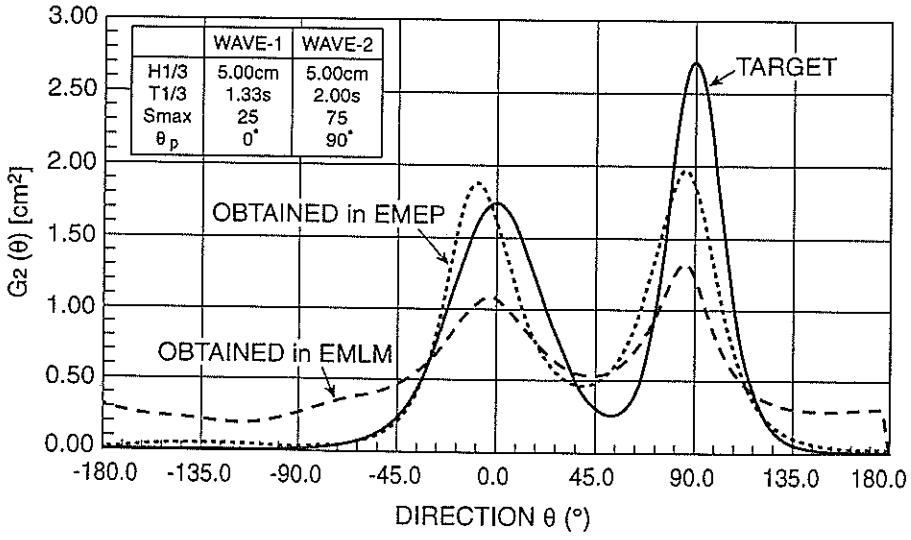

Figure 19 Comparison of two dimensional directional spectrum of measured and target double-peaked directional wave

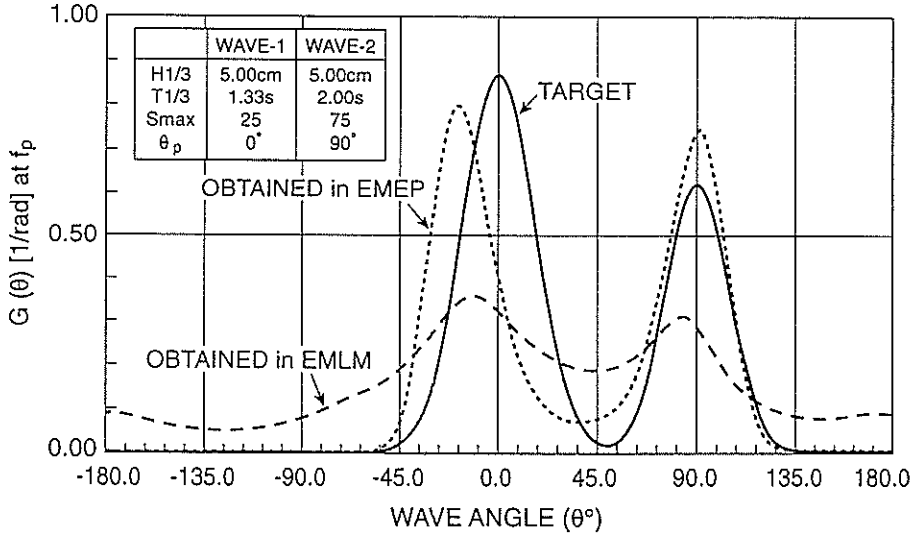

Figure 20 Comparison of directional function at fp of measured and target double-peaked directional wave

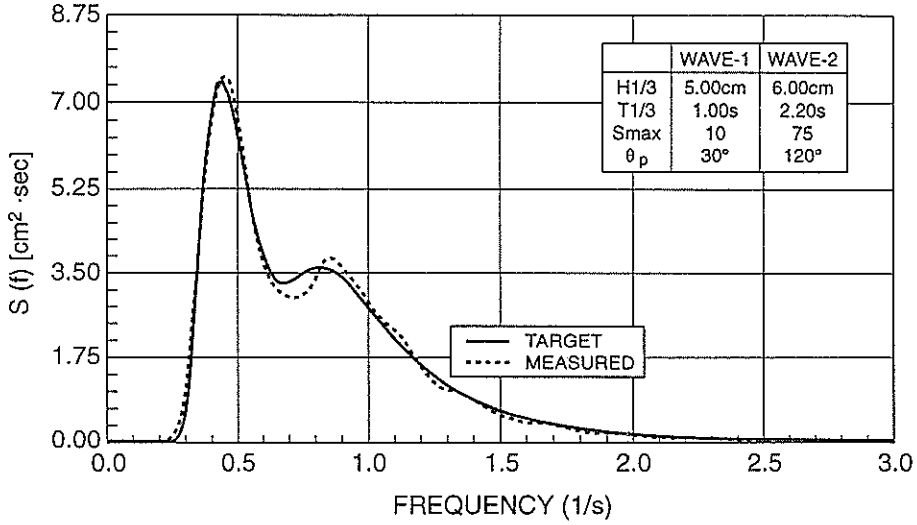

Figure 21 Comparison of frequency spectrum of measured and target double-peaked directional wave

3.5 Generated long period wave and solitary wave from second surface

(1) Long period wave

In order to investigate the efficiency and stability of floating structures in ocean, the reproduction of long period waves is important. **Figure 22** shows the comparison of the obtained and target frequency spectrum of uni-directional random waves including the long period wave components. The uni-directional waves were generated from the second face and the first face was employed as a fixed guide wall. In the figure, the solid line represents the target frequency spectrum.

The target spectrum has a constant level in the long period wave range. The broken line represents the experimentally obtained spectrum. The obtained spectrum agrees well with the target even in the range of long period waves. Therefore, the generator with a long stroke is expected to be applied to genarate the uni-directional wave condition with free long period wave components in the experimental basin.

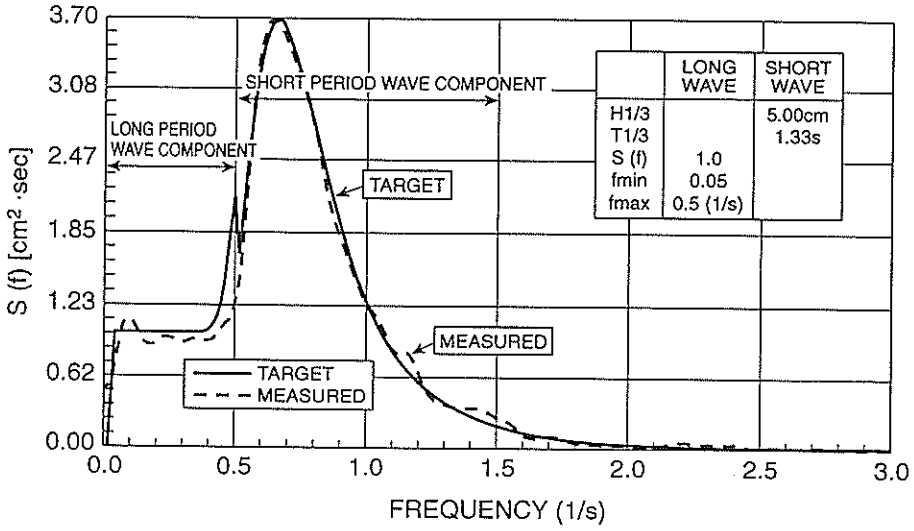

Figure 22 Measured and target wave frequency spectrum including short and long period wave component

(2) Solitary wave

The solitary wave is employed to represent tsunami wave offshore. The following equation for water particle velocity of solitary wave at water furface (Mei, 1989) was given to the synthesized wave paddle velocity signals:

$$\left.\begin{aligned} u|_{paddle} &= \sqrt{gh}\,\frac{H}{h}\left(1-\frac{5}{4}\frac{H}{h}\right)\mathrm{sech}v' \\ &\quad +\sqrt{gh}\,\frac{5}{4}\left(\frac{H}{h}\right)\mathrm{sech}v' \\ v' &= \sqrt{\frac{3H}{4h}}\left(1-\frac{5}{8}\frac{H}{h}\right)(-ct) \\ c &= \sqrt{gh}\left(1+\frac{1}{2}\frac{H}{h}-\frac{3}{20}\left(\frac{H}{h}\right)^2\right) \end{aligned}\right\} \qquad (7)$$

Figure 23 shows the recorded wave profile at the center part in the basin. The obtained maximum surface elevation from the sea level is about 15cm and it is the same to the target one. Therefore, the solitary wave needed for the reproduction of tsunami can be reproduced in the plane basin using the dual-face serpent type wave generator.

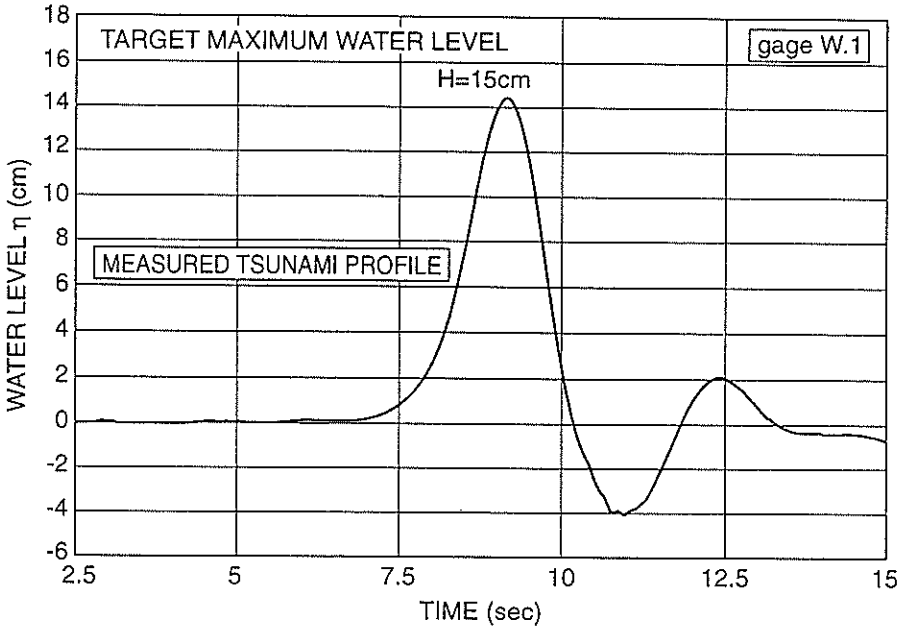

Figure 23 Mesaure profile of solitary wave

3.6 Continuous variation of principal wave direction

The principal wave direction of target waves is usually fixed to a single direction in a series of experiments. However, the wave propagating direction in the sea is sometimes dramatically changed even in a storm because of the rapid traveling of atomospheric low pressures. The variation of wave propagating direction has large influences to the stability of beach. And the motion of moored large floating structure is determined by wave direction. The model test with variable wave directions are very important to evaluate the safety factor of the floating structure.

We adopt a simple mechanical system for the continuous wave directional change system in the generation. **Figure 24** shows the image of synthesizing generation signals η_1 for **wave 1** and η_2 for **wave 2** each with different direction. In the continuous generation time, the transit interval time is adopted. In the operation, we employed 6sec and 10sec as the transit interval time in case of regular and irregular waves respectively. During the transit interval time, the signal η_1 for **wave–1** is transformed to η_2 for **wave–2.** The generation signal from the computer depends on the operation mode. The displacement of paddle and the target water elevation are employed as the signal for the case of position control and active absorption method respectively. The indication η represents such generation signal from the computer. The transit interval starts at t_s and the transit is completed at t_c. The wave representative signal η is given by,

$$\left.\begin{aligned} \eta(t)&=\eta_1(t) && (t\leqq t_s)\\ \eta(t)&=\left(1-\frac{t-t_s}{t_c}\right)\eta_1(t)+\frac{t-t_s}{t_c}\eta_2(t) && (t_s<t\leqq t_c)\\ \eta(t)&=\eta_2(t) && (t_c<t) \end{aligned}\right\} \qquad (8)$$

where $\eta 1(t)$ and $\eta 2(t)$ is corresponding to **wave 1** and **2** signals respectively.

Figure 25 shows the arrangemnet of verification experiment for continuous wave angle variation. In the experiment, sixteen wave sensors are employed to obtain the regular wave propagating angle. At sensors of **W4, W6, W14,** the wave gage array are installed employing the sensor for regular wave measurement as the center of the array to measure the wave directional spectrum. These three arrays are employed to determine the

propagating wave angle of uni−directional waves. In the experiment, regular and uni−directional wave are employed because the variation of wave propagating angle is clearly recognized. **Figure 26** shows the image to determine the regular wave direction employing the neighboring two sensors. The distance of two sensors is *DX*. The wave profile shown in the upper figure may be obtained at **Point.1** and **Point.2** in the lower figure with the phase lag represented by Δt. Considering wave celerity c, the angle θ is estimated in the following equation.

$$DX\sin\theta=c\Delta t \tag{9}$$

In the analysis, three trials employing $\Delta t1$, $\Delta t2$ and $\Delta t3$ are done to obtain the averaged values. For the generation, one signal is generated for 60sec and the next signal is generated with the transit time of 6s. The experimental water depth is 70cm.

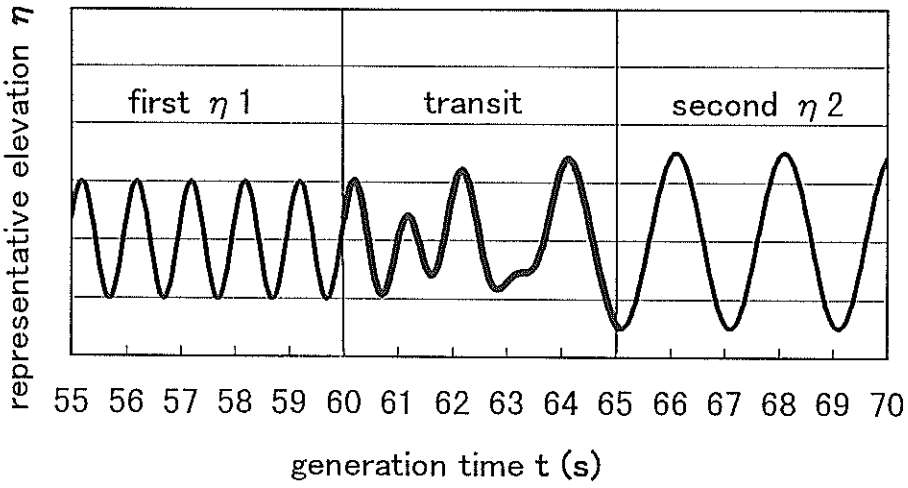

Figure 24 Image of wave signal profile variation with different propagating angle

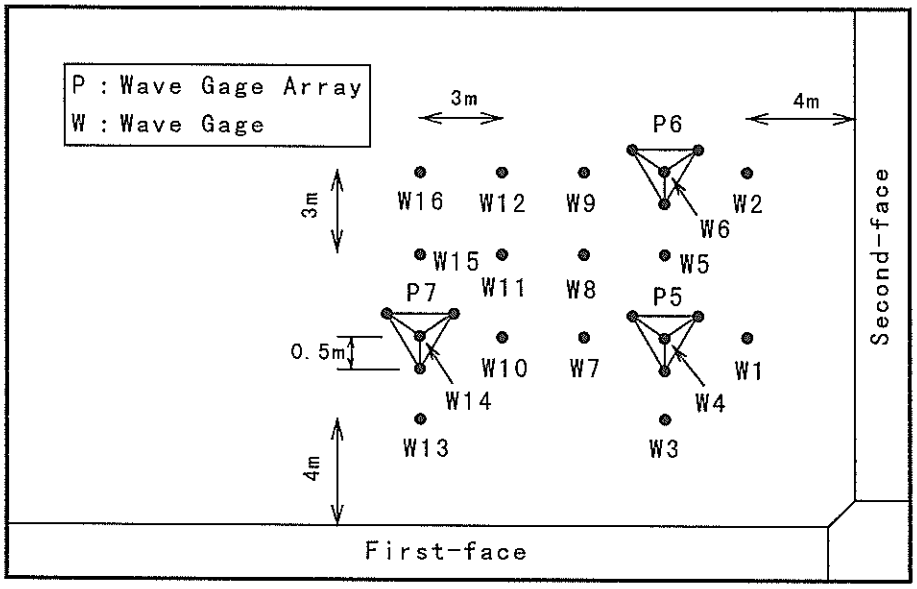

Figure 25 Location of wave gage and array for measurement of wave directional variation

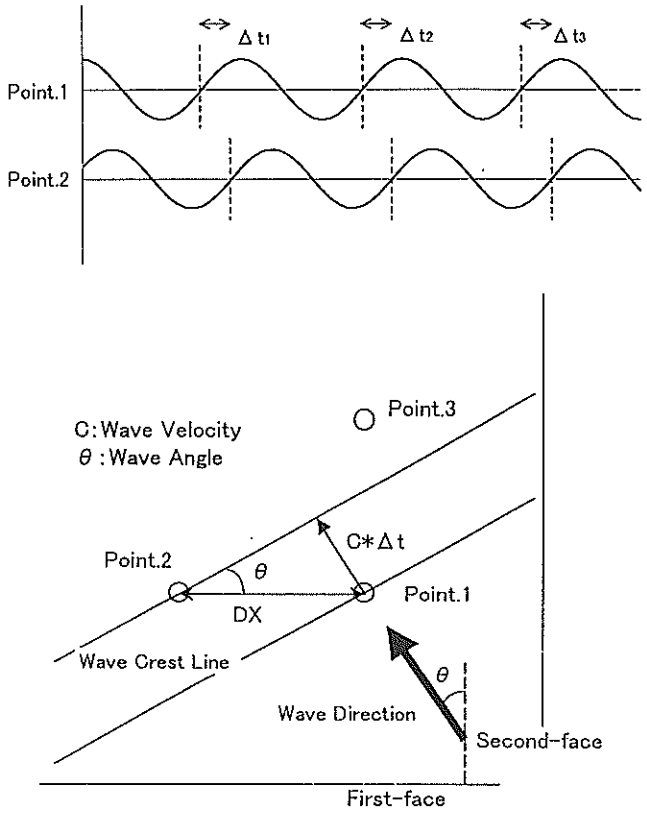

Figure 26 Determination of wave propagating angle from measured phase difference

Figure 27 shows the obtained wave angle at each steady time for each angle. In the experiment, the regular wave train with the angle of 0, 15, 30, 45, 60, 75 and 90° are continuously generated with the transit interval time of 6sec. The figures show the analysed wave angle 30sec after the completion of transit. The small numbers in the basin indicate the wave heights. In the figure (1) for $\theta = 0^\circ$, the wave angles at each position are same and they indicates the target of 0°. In the figure (2), (3) and (4), the wave angles represented by the vectors quite agree with the target angles. Even for the large angle cases for the figure (6) and (7), the wave angle represented in vectors agrees with the target vectors. Therefore, the wave angle can be changed continuously with good accuracy. The influences of transit signal are not measured after the intervals.

The similar experiments are carried out for the irregular wave cases. **Figure 28** shows the comparison of target and measured frequency spectrum for each wave direction. The transit time is 10sec between the different wave signals. The data length for one case of uni-directional waves is 410sec and the sampling time is 0.05sec. For the case of Fig.28(1), the gap among the measured spectrum at different arrays are very small. The three frequencies spectrum measured at diffrent positions agrees well to target at each point. For the case of $\theta_p = 30^\circ$, the energy level obtained at the different array represents the wide variety. The agreement among the frequency level are wider than in the case of $\theta_p = 0^\circ$.

Figure 29 shows the analysed directional spectrum for the uni-directional waves after the transit time. We investigate the enegy spreading influenced by the signal in the tarnsit intervals. For the all cases with the angle of $\theta_p = 0$, 30, 45, 60 and 90°, the directional spectrum represented in the contour map shows the high peaks at the target wave propagating angles. Therefore, the uni-directional waves with the target wave angle are generated without any influences of transit interval. The dual face serpent type wave generator is applicable with good accuracy to change the wave direction during one continuous operation time.

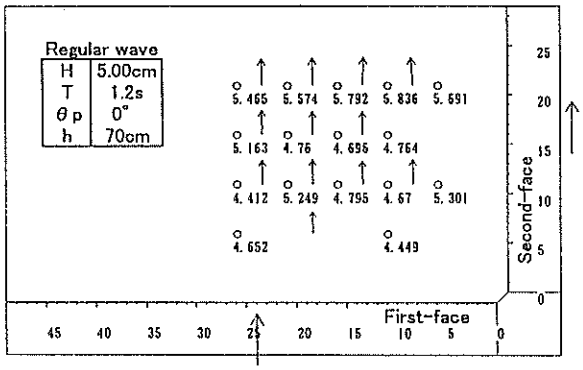

(1) Wave Direction(θ p)=0°

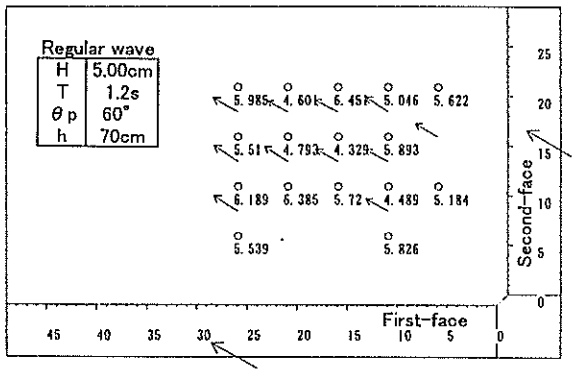

(5) Wave Direction(θ p)=60°

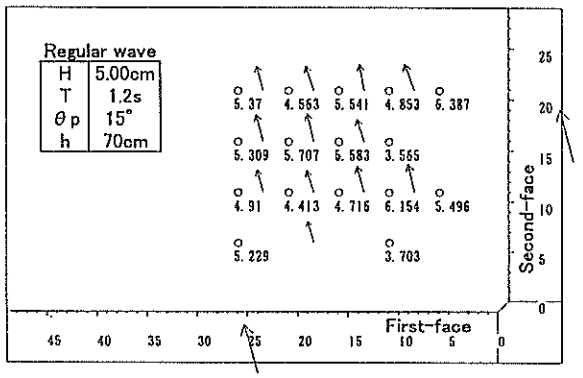

(2) Wave Direction(θ p)=15°

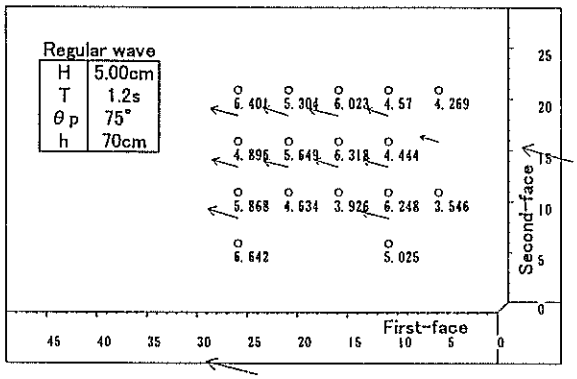

(6) Wave Direction(θ p)=75°

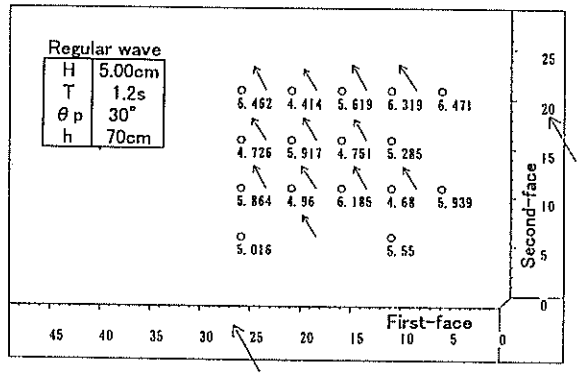

(3) Wave Direction(θ p)=30°

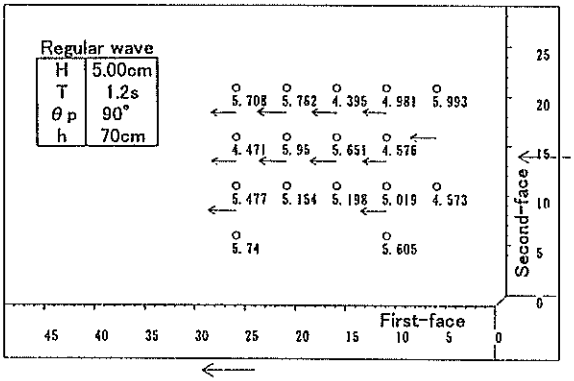

(7) Wave Direction(θ p)=90°

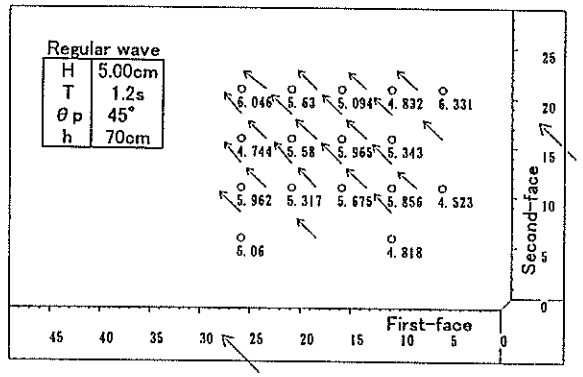

(4) Wave Direction(θ p)=45°

Figure 27 Spatial variation of wave angle obtained from phase lag

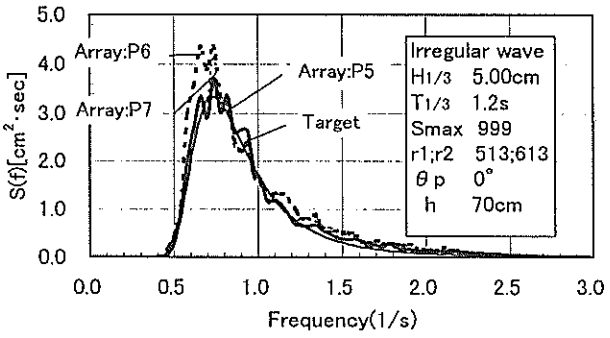

(1) Wave Direction (θ p) =0°

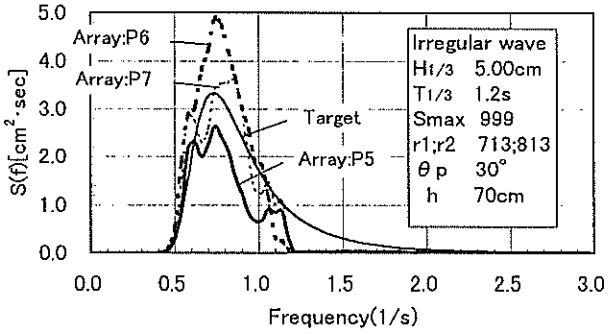

(2) Wave Direction (θ p) =30°

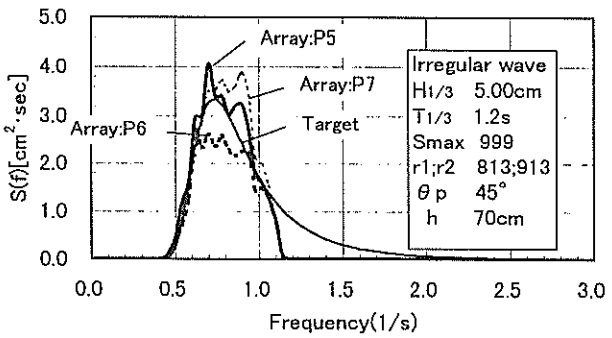

(3) Wave Direction (θ p) =45°

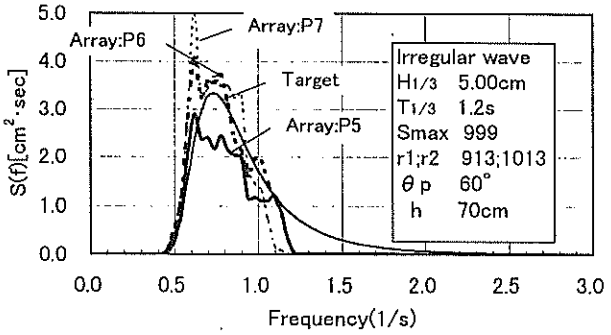

(4) Wave Direction (θ p) =60°

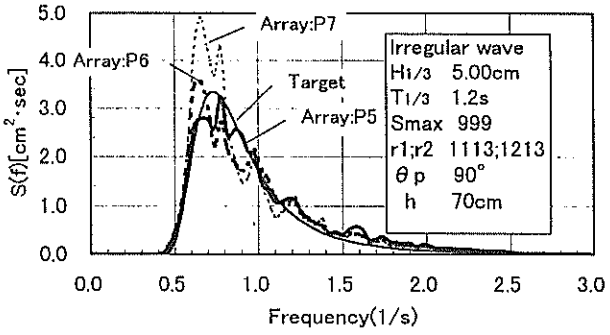

(5) Wave Direction (θ p) =90°

r1; Initial Random Number of Frequency
r2; Initial Random Number of Direction

Figure 28 Comparison of target and measured frequency spectrum during change of wave angle

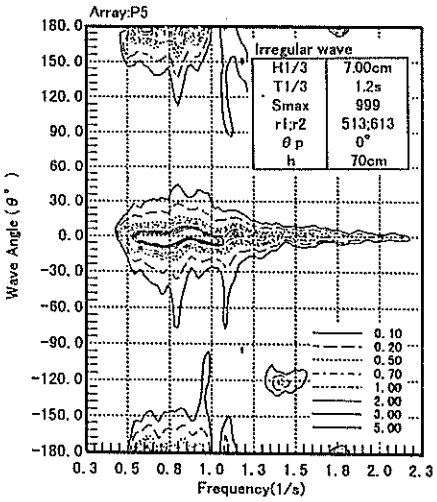

(1) Wave Direction(θ p)=0°

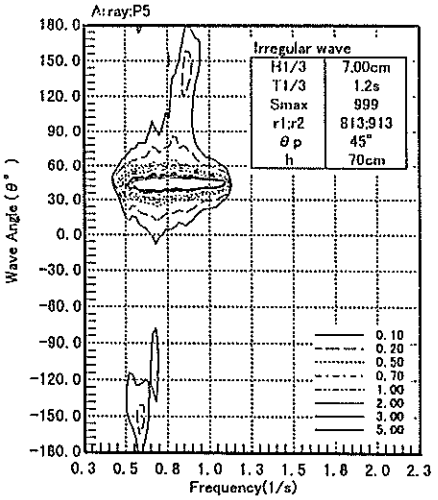

(3) Wave Direction(θ p)=45°

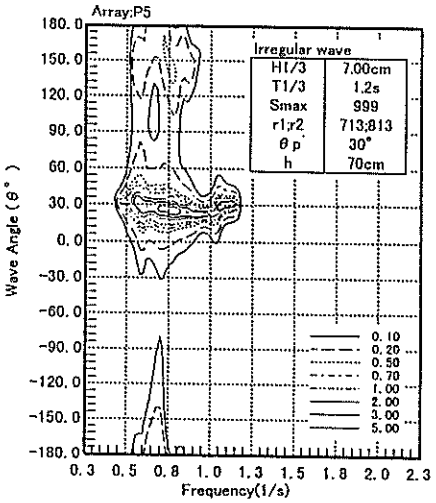

(2) Wave Direction(θ p)=30°

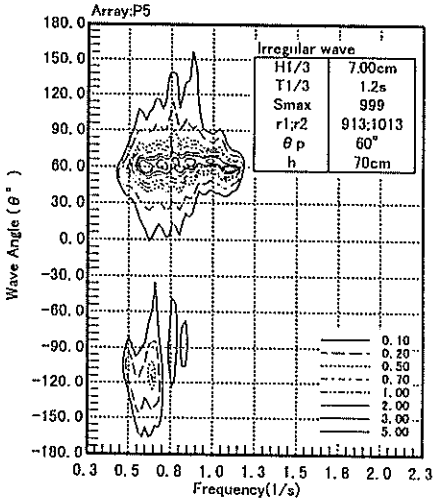

(4) Wave Direction(θ p)=60°

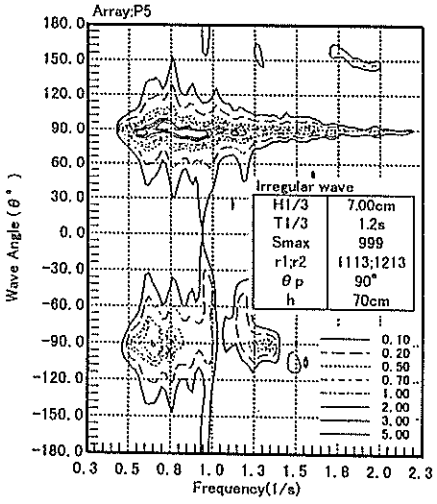

(5) Wave Direction(θ p)=90°

r1: Initial Random Numbar of Frequency
r2: Initial Random Number of Direction

The directional spectrum are obtained in EMLM

Figure 29 Directional spectrum after transit interval

4. Conclusions

A new type of directional wave generator has been developed to produce the large effective test area and to reproduce waves with the double-peaked directional spectrum composed of swell and wind wave components. It is named "Dual face serpent-type directional wave generator" because the generator is composed of double generator faces and operation modes. The first and second face consists of 50 and 30 driving shafts respectively. The width of each paddle between the two neighboring shafts is 60cm. The following results have been derived from the theoretical and experimental investigation;

(1) The active absorption system of the generator effectively works and the oblique incident waves are absorbed almost perfectly in the generator face.

(2) In the center area of the basin, the target directional waves with the normal and oblique principal wave direction are reproduced with good accuracy employing the multi-face operation mode.

(3) The dual-face directional random wave maker is applicable to enlarge the effective test area. The generator can make the whole area of the basin effective when the principal wave direction becomes 45°. The directional spectrum experimentally obtained at any measurement points in the basin agree well with the target for the case of $\theta_p = 45°$.

(4) The generator is applicable to reproduce long period waves and solitary waves.

(5) During operation with a continuous signal, the generator is capable to vary the wave propagating angle to any direction.

(Received on September 28,1998)

References

Funke E.R. and M.D.Miles (1987), "Multi-directional wave generation with corner reflectors," *Technical Rep. of National Res. Council Canada*, TR-HY-021,17p.

Goda Y.(1987),"Standard spectra and statistics of sea waves derived by numerical simulation", *Proc. 34th Japanese Conf. on Coastal Engineering*, pp.131-135.

Goda Y.(1985), "Random seas and design of maritime structures," *University of Tokyo Press*, pp.27-33.

Goda Y.and Y.Suzuki (1975), "Computation of refraction and diffraction of sea waves with Mitsuyasu's directional spectrum," *Technical Note of Port and Harbour Res. Inst.*, No.230, 45p.

Hashimoto N.,T.Nagai and T.Asai (1994), "Extension of maximum entropy principle method(MEP) for estimating directional wave spectrum," *24th Inter. Conf. Coastal Engineering*, Vol.1, pp.232-246.

Hiraishi,T and T. Takayama(1993), "A new approach to extension of effective test area in multi-directional wave basin," *Proc.25th Congress, International Association of Hydraulic Research*, C-3-3, pp.88-95.

Hiraishi T., T.Kanazawa and H.Fujisaku (1995), "Development of multi-face directional random wave maker, " *Proc. 5th Inter. Offshore and Polar Engi. Conf.*,Vol.3, pp.26-33.

Hiraishi T., Y.Atsumi, S.Sekiguchi and T.Kawaguchi (1997a), "Observation of long period wave and ship motion in Tomakomai-port, " *Proc. 7th Inter. Offshore and Polar Engi. Conf.*, Vol.3, pp.546-551.

Hiraishi T.(1997b), "Characteristics of long-period waves observed in a port," *Proc. 7th Inter. Offshore and Polar Engi. Conf.*, Vol.3, pp.254-258.

Hiraishi T.(1998), "Observed frequency spectrum of long period waves," *Proc. 8th Inter. Offshore and Polar Engi. Conf.*, Vol.3, pp.77-83.

Hirakuchi ,H.,R.Kajima,T.Shimizu and M.Ikeno (1992), "Characteristics of absorbing directional wavemaker, " *25th Inter. Conf. Coastal Engineering*, Vol.1, pp.281-294.

Isobe M.(1988) . "Measurement of wave direction," Chapter 3, *Nearshore Dynamics and Coastal Processes*, edited by K.Horikawa, University of Tokyo Press, pp.407-422.

Ito K.,H.Katsui,M.Mochizuki and M.Isobe (1996), "Non-reflected multi directional wave maker theory and experiments of verification," *Proc. 25th Inter. Conf. Coastal Engineering*, Vol.4, pp.443-456.

Mei C.C.(1989), "The applied dynamics of ocean surface waves," World Scientific, pp.541-543.

Nagai T.,N.Hashimoto and T.Asai (1993), "On the properties of the directional wave spectra observed in deep seas -1st report : The field observation off Iwaki-," *Report of the Port and Harbour Research Institute*, Vol.32, No.2, pp.45-114.

Takayama, T.(1982), "Theoretical properties of oblique waves generated by serpent-type wave-makers," *Rep. the Port and Harbour Research Institute*, Vol.21, No.2, pp.3-48.

Takayama T.and T.Hiraishi (1989), "Reproducibility of directional random waves in laboratory wave simulation," *Rept. of Port and Harbour Res. Inst.*,Vol.28,No.4,pp.3-24.

Takayama T.,N.Ikeda and Y.Kosugi (1991), "Hydraulic model tests on directional random wave transformation in Kamaishi bay, " *Report of the Port and Harbour Research Institute*, Vol.30, No.1, pp.69-136.

List of Symbols

b : width of generator segment
c : wave celerity
DX : distance between neiboring wave sensor
f : frequency
f_p : peak frequency
$G(\theta;f)$: directional function
$G_2(\theta)$: two dimensional directional spectrum
H : wave height
$H_{1/3}$: significant wave height
h : water depth
L : wave length
$S(f)$: frequency spectrum

$S(f;\theta)$: directional spectrum
S_{max} : angular spreading parameter
$T_{1/3}$: significant wave period
t : time
t_c : completion time of transit interval
t_s : start time of transit interval
Δt : phase lag
η : representative wave signal
θ : wave angle
θ_p : principal wave direction